Published in final edited form as:
Nat Immunol. 2020 March ; 21(3): 321–330. doi:10.1038/s41590-020-0596-6.

Spatiotemporal regulation of type I interferon expression determines the antiviral polarization of CD4+ T cells

Marco De Giovanni[1,2], **Valeria Cutillo**[1,2], **Amir Giladi**[3], **Eleonora Sala**[1,2], **Carmela G. Maganuco**[1], **Chiara Medaglia**[3], **Pietro Di Lucia**[1], **Elisa Bono**[1], **Claudia Cristofani**[1], **Eleonora Consolo**[1,2], **Leonardo Giustini**[1], **Alessandra Fiore**[2], **Sarah Eickhoff**[4], **Wolfgang Kastenmüller**[4], **Ido Amit**[3], **Mirela Kuka**[#1,2,‡], **Matteo Iannacone**[#1,2,5,‡]

[1]Division of Immunology, Transplantation and Infectious Diseases, IRCCS San Raffaele Scientific Institute, 20132 Milan, Italy

[2]Vita-Salute San Raffaele University, 20132 Milan, Italy

[3]Department of Immunology, Weizmann Institute of Science, Rehovot, Israel

[4]Institute of Systems Immunology, Wurzburg, Germany

[5]Experimental Imaging Center, IRCCS San Raffaele Scientific Institute, 20132 Milan, Italy

[#] These authors contributed equally to this work.

Abstract

Differentiation of $CD4^+$ T cells into either follicular helper T (T_{FH}) or type 1 helper T (T_H1) cells influences the balance between humoral and cellular adaptive immunity, but the mechanisms whereby pathogens elicit distinct effector cells are incompletely understood. Here, we analyzed the spatiotemporal dynamics of $CD4^+$ T cells during infection with recombinant vesicular stomatitis virus (VSV), which induces early, potent neutralizing antibodies or recombinant lymphocytic choriomeningitis virus (LCMV), which induces a vigorous cellular response, but inefficient neutralizing antibodies, expressing the same T cell epitope. Early exposure of dendritic cells to type I interferon (IFN), which occurred during infection with VSV, induced the production

[‡]Correspondence to: kuka.mirela@hsr.it, iannacone.matteo@hsr.it.

Accession codes
RNA-seq data that support the findings of this study have been deposited in the Gene Expression Omnibus (GEO) under accession code GSE130009.

Data and materials availability
All data is available in the main text or the supplementary materials.
RNA-seq data that support the findings of this study have been deposited in the Gene Expression Omnibus (GEO) under accession code GSE130009.

Author contributions
M.D.G., V.C. and M.K. designed and performed experiments, analysed data, performed the statistical analyses and drafted the manuscript; E.S., C.G.M., P.D.L., E.B., C.C., E.C., L.G. and A.F. performed experiments and analysed data; A.G., C.M. and I.A. performed the NICHE-seq and scRNA-seq analyses and prepared the related figures; S.E. and W.K. performed the XCR1-DTR experiments and analysed data; M.K. provided funding, conceptual advice and supervision; M.I. designed and coordinated the study, provided funding, and wrote the paper.

Competing interests
Authors declare no competing interests.

Europe PMC Funders Author Manuscripts

of the cytokine IL-6 and drove T_{FH} cell polarization, while late exposure to type I IFN, which occurred during infection with LCMV, did not induce IL-6 and allowed differentiation into T_H1 cells. Thus, tight spatiotemporal regulation of type I IFN shapes antiviral $CD4^+$ T cell differentiation, and might instruct vaccine design strategies.

$CD4^+$ T cells are key players in adaptive immune responses against pathogens. After priming in secondary lymphoid organs (SLOs), antigen-specific $CD4^+$ T cells undergo clonal expansion and differentiation into specialized effector T cell subsets. Viral infection may result in the generation of follicular helper T cells (T_{FH} cells) and type 1 helper T cells (T_H1 cells) [1,2]. T_{FH} cells, which express the transcription factor Bcl-6, migrate into the B cell follicles where they promote the formation of high-affinity neutralizing antibodies[3,4]. T_H1 cells, which express the transcription factor T-bet[5], promote the activation of macrophages and $CD8^+$ T cell responses. As such, T_{FH} and T_H1 cell subsets contribute to adaptive immune responses by specifically supporting humoral or cellular immunity, respectively.

Although humoral or cellular immunity can be found in a state of “competitive coexistence”[6], one response usually emerges as dominant after viral infection and is responsible for most of the antiviral activity. Viruses that induce direct cell damage (cytopathic viruses), such as the vesicular stomatitis virus (VSV), typically induce early, potent neutralizing antibody responses[7], while non-cytopathic viruses, such as the lymphocytic choriomeningitis virus (LCMV), usually elicit robust cellular responses, but weak and inefficient neutralizing antibody responses[7]. The relative inefficiency of non-cytopathic viruses to induce neutralizing antibodies has been attributed, among other factors, to the properties of viral surface proteins, the frequency of germline-encoded immunoglobulin variable regions, the $CD8^+$ T cell-induced immunopathological changes in secondary lymphoid organs and the inflammatory monocyte-mediated suppression of B cells[7,8]. Here, we investigated whether $CD4^+$ T cell polarization had a role in the dichotomous response to VSV and LCMV and characterized the spatiotemporal dynamics of the differentiation of antiviral $CD4^+$ T cells. We found that $CD4^+$ T cells differentiated mostly to T_{FH} cells upon infection with VSV and mostly to T_H1 cells upon infection with LCMV. Regardless of the differentiation outcome, priming of $CD4^+$ T cells occurred in the outer paracortex and in the interfollicular areas of the lymph nodes in both infections. The dichotomous T cell differentiation could not be explained by distinct cellular composition of the priming niches. Instead, the spatiotemporal regulation of type I interferon (IFN) expression determined whether dendritic cells (DC) in the lymph node produced the cytokine IL-6 and, consequently, shaped antiviral $CD4^+$ T cell polarization.

Results

VSV and LCMV induce distinct antiviral $CD4^+$ T cell polarization

First, we compared $CD4^+$ T cell polarization upon VSV or LCMV infection in C57BL/6 mice. We adoptively transferred naïve VSV-specific (Tg7)[9] or LCMV-specific (SMARTA)[10] transgenic $CD4^+$ T cells into C57BL/6 mice 24 h before subcutaneous intra-footpad infection with VSV Indiana (VSV Ind) or LCMV WE, respectively. $CD4^+$ T cell

Europe PMC Funders Author Manuscripts

polarization into Bcl-6^{+} CXCR5^{+} T_{FH} cells and T-bet^{+} CXCR5^{-} T_H1 cells was analysed at 3, 5, 7 and 14 days after infection in the footpad-draining popliteal lymph nodes (dLNs) (Extended Data 1a). On day 5 after VSV infection, >40% of Tg7 T cells differentiated into T_{FH} cells, with little or no differentiation into T_H1 cells (Fig. 1a); at the same time point, >80% of SMARTA T cells were T_H1 cells, and <15% became T_{FH} cells (Fig. 1a). This pattern of CD4^{+} T cell polarization during VSV and LCMV infections was also observed when we analysed the endogenous CD44^{hi}CD4^{+} T cell response in dLNs of mice subcutaneously infected with different viral strains (VSV Ind, VSV New Jersey, LCMV Armstrong, LCMV WE and LCMV clone 13) (Extended Data 1b, c), and it occurred independently of the route of infection (intrafootpad and intravenous infections) (Extended Data 1d) and the size of viral inoculum (10^2-10^7 pfu or ffu/mouse) (Extended Data 1e).

TCR signal strength influences CD4^{+} T cell fate, with high-affinity antigen recognition associated to increased induction of T_{FH} cells [11]. To test whether the distinct CD4^{+} T cell differentiation during the VSV and LCMV infection was due solely to different TCR binding affinities, we infected C57BL/6 mice subcutaneously with recombinant VSV (rVSV) and LCMV (rLCMV) expressing glycoproteins containing the LCMV gp61-80 epitope recognized by SMARTA CD4^{+} T cells[12,13]. On day 5, >40% of SMARTA CD4^{+} T cells differentiated into T_{FH} cells upon infection with rVSV, while >60% of cells became T_H1 cells upon infection with rLCMV (Fig. 1b, c and Extended Data 1f, g), indicating that features of the viral backbone dictated the cell fate of the CD4^{+} T cells, independently of the TCR affinity.

We next tested the localization and dynamic behaviour of CD4^{+} T cells in the LN by confocal immunofluorescence histology and intravital multiphoton microscopy (IVM). We imaged the draining LNs of wild-type mice transferred with CD4^{+} T cells from Tg7 x β-actin-GFP or SMARTA x β-actin-GFP mice on day 3 post-infection with VSV Ind, rVSV or rLCMV. At this time point, we detected Tg7 or SMARTA T cells in the B cell follicles following infection with either VSV Ind or rVSV, respectively (Fig. 1d, e); by contrast, SMARTA T cells in rLCMV-infected mice were confined outside the B cell follicles (Fig. 1d, e). The imaged Tg7 or SMARTA T cells had a higher velocity and higher meandering index, an indicator of track straightness, in mice infected with either VSV Ind or rVSV, respectively, than SMARTA cells in mice infected with rLCMV (Fig. 1f, g, Extended Data 2a, b and Supplementary Movie 1). These data indicated that VSV and LCMV induced distinct antiviral CD4^{+} T cell polarization and *in vivo* dynamic behaviour, independently of viral strain, viral dose, infection route and TCR signal strength.

Characterization of the antiviral CD4^{+} T cell priming niche

Next, we characterized the precise location in the LN where priming and differentiation of the antiviral CD4^{+} T cell took place. CD4^{+} T cell priming is thought to happen within the first two days upon antigen administration in the outer paracortex and interfollicular areas of LNs[14–17]. Consistent with this, 48 h post-infection with rVSV or rLCMV, SMARTA CD4^{+} T cells had upregulated the activation markers CD69 and CD25 (Extended Data 2c, d) and migrated to the outer paracortex and interfollicular areas of the infected LNs (Fig. 2a, b, Extended Data 2e and Supplementary Movie 2), where they started to form clusters (Fig. 2a,

c, Extended Data 2f and Supplementary Movie 2). We refer to these areas as $CD4^+$ T cell 'priming niches' hereafter. To test whether the cellular and molecular composition of the niche supporting $CD4^+$ T cell priming differed between the rVSV or rLCMV infections, we used NICHE-seq, which combines photoactivation and single-cell RNA-sequencing (scRNA-seq) to spatially reconstruct immune niches[18]. We intravenously transferred $CD4^+$ T cells from SMARTA x β-actin-CFP mice into transgenic mice ubiquitously expressing a photoactivatable green fluorescent protein (PA-GFP)[19]; we then photoactivated areas in the dLNs containing SMARTA $CD4^+$ T cell clusters (i.e. in the outer paracortex and interfollicular areas) on day 2 post-infection with rVSV or rLCMV and single-cell sorted 2406 photoconverted total GFP^+ endogenous cells (Fig. 2d, e). scRNA-seq indicated that B cells and NK cells were over-represented in the samples from rVSV-infected mice, whereas $CD8^+$ T cells and $CCR2^+$ inflammatory monocytes were enriched in the samples from rLCMV-infected mice (Fig. 2e, f; cell subsets were identified based on their gene expression signatures, see Methods). Confocal microscopy indicated the presence of Ag-specific B cells, $CX3CR1^+CCR2^+$ cells, Ag-specific $CD8^+$ T cells and $NKp46^+$ cells in the $CD4^+$ T cell-priming niches (Extended Data 3a-d).

B cells are required for the later stages of differentiation into T_{FH} cells [3]. To test whether a higher number of B cells in the $CD4^+$ T cell-priming niche in the VSV-infected mice drove differentiation into T_{FH} cells, we used VI10Yen mice, in which B cells express a transgenic BCR specific for an irrelevant antigen (VSV Ind glycoprotein)[20]. Adoptively transferred SMARTA $CD4^+$ T cells differentiated into T_{FH} cells and homed to the B cell follicles similarly in wild-type or VI10Yen mice after infection with rVSV (Fig. 2g and Extended Data 4a), indicating that Ag-specific B cells were not needed for the initial differentiation of $CD4^+$ T cells. NK cells were reported to curtail virus-specific $CD4^+$ T cell responses, including T_{FH} cell responses, during chronic virus infection[21]. However, depletion of $NKp46^+$ cells, including NK cells, in NKp46-Cre x Rosa26-iDTR mice [22,23] injected with diphtheria toxin, indicated NK cells were dispensable for early SMARTA $CD4^+$ T cell differentiation upon rVSV or rLCMV infection (Extended Data 5a-c). Immunopathological changes in secondary lymphoid organs or direct killing of B cells by $CD8^+$ T cells can subvert B cell responses[8,24–26]. The use of Cor93 Tg recipient mice, in which T cells bear a TCR specific for an irrelevant antigen (the hepatitis B virus core protein)[27], indicated that Ag-specific $CD8^+$ T cells were not required for the early polarization of SMARTA $CD4^+$ T cells upon rVSV or rLCMV infection (Fig. 2h and Extended Data 4b). The recruitment of $CCR2^+$ inflammatory monocytes to the LCMV-infected LNs was shown to hinder LCMV-specific B cell responses[8,28]. However, *Ccr2*$^{-/-}$ recipient mice, in which monocytes cannot migrate to infected LNs[28,29], were indistinguishable from wild-type mice in their ability to support early SMARTA $CD4^+$ T cell differentiation upon rVSV or rLCMV infection (Fig. 2i and Extended Data 4c).

Priming of naïve $CD4^+$ T cells within LNs is mediated by mature conventional dendritic cells (cDC), which present antigen and deliver costimulatory stimuli and cytokines[14,15,17,30]. cDCs were detected in the T_{FH} cell and T_H1 cell priming niches by NICHE-seq (Fig. 2e, f), but the relative paucity of these cells within the photoactivated cells prevented their detailed phenotypic characterization. The membrane receptor ICOSL is sensitive to ICOS-induced shedding during interactions with activated $ICOS^{hi}$ T cells[31]. To determine the DC subsets

that interacted with the $CD4^+$ T cells upon VSV or LCMV infection, we measured the expression of ICOSL on $CD11c^+MHCII^{hi}$ DCs in rVSV- or rLCMV-infected mice treated with a blocking antibody against ICOS, as an indirect indicator of the interaction between LN DCs and cognate T cells. In both rVSV- and rLCMV-infected mice, $CD11c^+MHCII^{hi}CD11b^+$ cDC2, but not $CD11c^+$ $MHCII^{hi}CD8^+$ cDC1, had increased expression of ICOSL (Extended Data 5d, e), suggesting that interactions between cDC2 and cognate $CD4^+$ T cells drive the differentiation of both T_{FH} and T_H1 cells. In addition, SMARTA $CD4^+$ T cells transferred into XCR1-DTR mice, in which cDC1s were depleted by diphtheria toxin injection starting 2 days before infection, differentiated normally into T_{FH} or T_H1 cells upon rVSV or rLCMV infection, respectively (Extended Data 5f). Thus, the differences in helper T cell polarization observed during the infection with VSV and LCMV were due to priming by DC subsets other than cDC1, possibly exposed to a different local cytokine milieu.

Spatiotemporal regulation of type I IFN expression determines $CD4^+$ T cell polarization

Next, we analysed the transcriptome of the cells in the photoactivated $CD4^+$ T cell priming niche of rVSV- and rLCMV-infected mice. NICHE-seq analysis indicated an increased type I IFN signature in cells isolated from the $CD4^+$ T cell-priming niche of rLCMV-infected mice compared to cells from the $CD4^+$ T cell-priming niche of rVSV-infected mice on day 2 post-infection (Fig. 3a). Although sensing of type I IFN is known to influence $CD4^+$ T cell polarization, the effect of type I IFN on the activation and differentiation of antiviral $CD4^+$ T cells remains ill defined, with conflicting reports, possibly depending on the context of infection. Kinetic analysis of IFN-α2, IFN-α5, IFN-α6, IFN-α7, IFN-α9, IFN-α12, IFN-α13, IFN-α14, IFN-β, and two representative IFN-stimulated genes (ISGs), ISG15 and OAS2, in total RNA isolated from LNs at 4, 8, 16, 24 and 48 h post-infection with rVSV or rLCMV indicated that although the magnitude of type I IFN induction did not significantly differ between the rVSV or rLCMV infection, rVSV induced an earlier wave of type I IFN, which peaked at 8 h after infection, whereas rLCMV induced a delayed (24 h) and prolonged peak (Fig. 3b and Extended Data 6), possibly reflecting the different kinetics of the viral replication *in vivo* [28]. REX3 reporter mice express the red fluorescent protein (RFP) and the blue fluorescent protein (BFP) under the control of the promoters of the ISGs *Cxcl9* and *Cxcl10*, respectively [17]. We detected stronger expression of CXCL9-RFP and CXCL10-BFP in the outer paracortex, cortical ridge and interfollicular areas in the LNs of rVSV-infected REX3 mice compared to rLCMV-infected mice 12 h post-infection, corresponding to areas where the SMARTA $CD4^+$ T cells accumulated (Fig. 3c).

To test the effect of the two profiles of type I IFN induction on the differentiation of $CD4^+$ T cells, we transferred SMARTA $CD4^+$ T cells into wild-type mice and treated them with an antibody that blocks signalling through the type I IFN receptor (IFNAR1) 1 day before infection with rVSV or rLCMV. Whereas the $CD4^+$ T cells transferred in IFNAR1-blocked rLCMV-infected mice differentiated into T_H1 cells, induction of T_{FH} cells in the rVSV-infected mice was severely compromised, with transferred $CD4^+$ T cells differentiating into T-bet^+ $CXCR5^-$ T_H1 cell, which were excluded from B cell follicles and induced fewer germinal centre B cells and GP-specific IgG1 antibodies (Fig. 3d, e, Extended Data 7a, b, and Supplementary Movie 3), suggesting that type I IFN affected $CD4^+$ T cell polarization at early time points post-infection. Administration of the blocking Abs against IFNAR1 on

day 1 post-rVSV infection did not affect the differentiation of SMARTA cells into T_{FH} cells compared to untreated controls (Fig. 3f, Extended Data 7c), indicating that type I IFN sensing within the first 24 h post-infection was essential for the induction of T_{FH} cells. To assess whether an early wave of type I IFN increased the differentiation of T_{FH} cells in LCMV-infected mice, we injected poly(I:C), which binds TLR3 to induce type I IFN, simultaneously with rLCMV. On day 5 post-infection, we observed a significant increase in T_{FH} cell differentiation and a reduction in T_H1 cells in the LNs of poly(I:C)-treated mice compared to untreated mice (Fig. 3g). Together, these results indicate that early (<24 h) type I IFN sensing drives T_{FH} cell differentiation.

Early type I IFN sensing by DC and IL-6 are essential for T_{FH} cell differentiation

Type I IFN sensing by different cell types has been reported to influence $CD4^+$ T cell differentiation in a variety of experimental settings, with data pointing to either a stimulatory or inhibitory role in the polarization towards either T_{FH} and/or T_H1 cells [32]. To investigate the role of type I IFN receptor signalling in $CD4^+$ T cells, we adoptively transferred wild-type or *Ifnar1*$^{-/-}$ SMARTA $CD4^+$ T cells into wild-type recipients 1 day before rVSV infection. On day 5 post-infection, we observed no differences between wild-type and *Ifnar1*$^{-/-}$ SMARTA cell differentiation into T_{FH} or T_H1 cells (Fig. 4a), indicating that intrinsic type I IFN sensing by $CD4^+$ T cells is dispensable for $CD4^+$ T cell differentiation. We next investigated the role of type I IFN sensing in DCs, which had the most upregulated expression of ISGs in the $CD4^+$ T cell priming niche (Extended Data 8). Wild-type SMARTA $CD4^+$ T cells adoptively transferred into irradiated wild-type mice reconstituted with CD11c-Cre x *Ifnar1*$^{fl/fl}$ bone marrow 8 weeks before $CD4^+$ T cell transfer showed significantly impaired differentiation into T_{FH} cells on day 5 post rVSV infection (Fig. 4b), indicating that type I IFN sensing by DCs was essential for antiviral T_{FH} induction.

IL-6 is known to promote early T_{FH} differentiation[33,34] and its induction to be dependent on type I IFN[35]. Kinetic analysis of *Il6* expression in LNs of wild-type mice infected with either rVSV or rLCMV indicated that induction of *Il6* mRNA had an early peak (8 h post-infection) during VSV infection and a delayed (>16 h) and lower peak during LCMV infection (Fig. 4c), mirroring the type I IFN signature. *Ifnar1*$^{-/-}$ mice had no upregulation of *Il6* mRNA 8 h after rVSV infection (Fig. 4d), indicating the VSV-induced early expression of *Il6* required type I IFN sensing. Blocking IL-6 prior to, but not 24 hours after rVSV infection significantly impaired the induction of T_{FH} cells and the virus-specific antibody titres and increased the induction of T_H1 cells (Fig. 4e, Extended Data 9a, b), while it did not affect T helper cell polarization upon rLCMV infection (data not shown). These observations identified IL-6 as a critical early determinant of the differentiation of antiviral T_{FH} cells.

To determine whether type I IFN induced the expression of IL-6 on DCs, we assessed the composition and transcriptional state of DC subsets after early or late type I IFN sensing. scRNA-seq on 2179 quality-controlled (QC)-positive $CD11c^+$MHC-II^{hi} DCs sorted from the lymph nodes of wild-type or *Ifnar1*$^{-/-}$ mice at 8 h or 48 h post-infection with rVSV or rLCMV and unbiased analysis using the Metacell package[36] indicated that the $CD11c^+$MHC-II^{hi} DCs could be subsetted into migratory cDC2, cDC1, cDC2, monocyte-derived

DCs (moDCs) and a small subset of contaminant macrophages (Fig. 5a). Experimental conditions where type I IFN signalling is maximal (i.e. 8 h after rVSV infection and 48 h after rLCMV infection of wild-type mice compared to the same time points in *Ifnar1*$^{-/-}$ mice or 8 h after rLCMV infection) showed an enrichment of DC subsets (i.e. migratory cDC2 and moDCs) that can support T_{FH} cell differentiation (Fig. 5b)[37]. Furthermore, ISGs induced by type I IFN were upregulated in DCs from wild-type, but not from *Ifnar1*$^{-/-}$ mice, particularly in experimental conditions (8 h post-rVSV and 48 h post-rLCMV infection) where type I IFN signalling is maximal (Fig. 5c, d and Extended Data 10), indicating that DCs responded to type I IFN. Importantly, migratory cDC2 and moDCs produced *Il6* at 8 hours after rVSV infection of wild-type but not *Ifnar1*$^{-/-}$ mice (Fig. 5e); by contrast, after rLCMV infection, *Il6* mRNA had very low expression in migratory cDC2 and moDCs from wild-type and *Ifnar1*$^{-/-}$ mice even at 48 h post-infection, when other ISGs were maximally induced (Fig. 5e). Thus, DCs produced *Il6* and drove T_{FH} cell polarization in response to early (rVSV) but not late (rLCMV) type I IFN signalling.

Discussion

Here, we identified the tight spatiotemporal regulation of the expression of type I IFN as a critical determinant of CD4$^+$ T cell fate upon viral infection. When DCs were exposed to an early (<24 h) wave of type I IFN, they made IL-6, thus promoting the differentiation of T_{FH} cells and, consequently, enhancing humoral immunity; in contrast, when DCs were exposed to late type I interferon (>24 h), they no longer produced IL-6, and CD4$^+$ T cells differentiated into a non-T_{FH} cell fate. These results might explain why many non-cytopathic, slow-replicating viruses fail to induce or interfere with the generation of neutralizing antibodies[7,8].

The notion that type I IFN influences the differentiation of CD4$^+$ T cells is not without precedent [32]. However, its role in CD4$^+$ T cell polarization has remained controversial. While some studies have shown type I IFN promoted T_{FH} cell differentiation, others reported that type I IFN suppressed the formation of T_{FH} cells or induced T_H1 cells[32]. Our results suggested that the spatial and temporal regulation of type I IFN was critical for its effect on DCs, thus providing a potential explanation for the abovementioned conflicting results. The cellular source of type I IFN in VSV and LCMV infections is an interesting question, but unfortunately, one that is technically difficult to address because of the many isoforms of type I IFN and the lack of a sensitive, robust type I IFN reporter mouse that would allow for the unambiguous identification of cells producing small amounts of these cytokines[38,39]. VSV induces production of type I IFN in subcapsular sinus macrophages and plasmacytoid dendritic cells[40]. However, the relative contribution of each abovementioned lymph node cell type to the production of type I IFN after subcutaneous infection with LCMV or the recombinant viral strains used in this study are unknown[41]. Nevertheless, it is tempting to speculate that subcapsular sinus macrophages might be the critical cellular source of the early type I IFN response necessary for T_{FH} cell differentiation. Pertinent to this, it is worth noting that viral infections induce a relocalisation of subcapsular sinus macrophages to the inner follicular areas and towards the anatomical niche where antiviral CD4$^+$ T cell priming takes place [42].

Our data identify DCs as the necessary platform that integrates early type I IFN signalling to promote T_{FH} cell differentiation. Mechanistically, type I IFN is necessary for the induction of the T_{FH} cell-promoting cytokine IL-6[35]. Our scRNA-seq data identified subsets of DCs (migratory cDC2 and moDCs) that produced *Il6* mRNA in response to early, but not late, type I IFN. One experimental caveat is that we analysed DCs from the entire lymph node, rather than from the $CD4^+$ T cell priming niche, thus potentially underestimating the localized production of IL-6 by DCs. The relative contribution of DC-derived IL-6, compared to IL-6 from other cellular sources, in shaping antiviral $CD4^+$ T cell polarization remains to be determined.

We found that $CD4^+$ T cells that differentiated into T_{FH} cells after rVSV infection showed relatively high velocity and high meandering index, whereas $CD4^+$ T cells that differentiated into T_H1 cells after rLCMV infection were characterized by reduced mean speed and lower meandering index. The mechanistic explanations for these different motility behaviours remain elusive, and might potentially include intrinsic differences in motility between T_{FH} cells and T_H1 cells, differences in spatial constrains provided by the different anatomical niche they occupy (B cell follicles versus interfollicular and T cell areas), different adhesion molecule expression and different antigen levels.

Blockade of early type I IFN signalling or blocking of IL-6 resulted in reduced generation of T_{FH} cells and, consequently, in reduced antiviral antibody responses. Of note, whereas the main effect of type I IFN blockade was observed on antiviral IgG1 titres, IL-6 affected mostly the levels of antiviral IgG2b. The reason for this discrepancy is unknown but might lie with additional T-independent roles of IL-6 that affect B cell differentiation [43].

Although the data presented in this study linked T_{FH} cell differentiation to early type I IFN sensing by DCs, they do not fully explain the strong T_H1 cell differentiation observed during LCMV infection. In addition to a lack of early type I IFN and IL-6, as reported here, LCMV might promote T_H1 cell differentiation through the induction of T_H1 cell-polarizing cytokines, such as IL-12 and IFN-γ[44–46]. Although IL-12 is dispensable for T_H1 cell polarization upon LCMV infection[47,48], the role of other cytokines such as IFN-γ on antiviral $CD4^+$ T cell differentiation, its cellular source and its potential interference with IL-6 induction warrants further investigation.

In conclusion, we have characterized the cellular and molecular composition of the LN niches where $CD4^+$ T cell differentiation occurs, delineated the spatiotemporal dynamics of the ensuing T_H cell subsets and identified the tight spatiotemporal regulation of type I IFN expression as a critical regulator of antiviral $CD4^+$ T cell polarization. Our model predicts that if viruses induce an early wave of type I IFN (a situation that typically occurs with fast-replicating, highly cytopathic viruses that are controlled by neutralizing antibodies), this cytokine acts on migratory cDC2 and/or monocyte-derived dendritic cells to induce IL-6 (and possibly other T_{FH} cell-promoting cytokines), drive T_{FH} cell differentiation and ultimately enhance humoral immunity; by contrast, if type I IFN is induced later upon viral infection (a situation that is typical of slow-replicating, non-cytopathic viruses that are controlled by the $CD8^+$ T cell response), DCs no longer make IL-6 and T_H cell polarization

is biased towards non-T_{FH} cell fates such as T_H1 cells, which favour cellular immunity at the expense of B cell responses.

Methods

Mice

C57BL/6, CD45.1 (inbred C57BL/6), β-actin-CFP (B6.129(ICR)-Tg(CAG-ECFP)CK6Nagy/J), β -actin-GFP [C57BL/6-Tg(CAG-EGFP)1Osb/J], *Ccr2*$^{-/-}$ (B6.129S4-Ccr2tm1Ifc/J), Rosa26-ZsGreen [B6.Cg-*Gt(ROSA)26Sor*$^{tm6(CAG-ZsGreen1)Hze}$/J][49] and PA-GFP[19] mice were purchased from Charles River or from the Jackson Laboratory. LCMV-P14[50], SMARTA[10], Tg7[9], and *Ifnar1*$^{-/-}$[51] mice were obtained through the Swiss Immunological Mouse Repository (SwImMR, Zurich, Switzerland). Heavy chain knock-in and light chain BCR transgenic mice specific for VSV Indiana (VI10YEN[20]) were obtained through the European Virus Archive. BCR transgenic mice specific for LCMV WE (KL25) bred against b-actin–DsRed were described in [28]. Cor93 TCR transgenic mice (lineage BC10.3, inbred CD45.1), in which > 98% of the splenic CD8+ T cells recognize a Kb-restricted epitope located between residues 93–100 in the HBV core protein (MGLKFRQL), have been previously described[27]. XCR1-DTR-Venus, CD11c-cre and *Ifnar1*$^{fl/fl}$ have been previously described[52–54]. NKp46-Cre [22] mice were obtained from Eric Vivier. Rosa26-iDTR[23] mice were obtained from Marco Bacigaluppi. CX3CR1$^{GFP/+}$ [55] and CCR2$^{RFP/+}$ [56] mice were provided by I. Charo (University of California, San Francisco) by way of B. Engelhardt (University of Bern). Bone marrow chimeras were generated by irradiation of C57BL/6 mice with ~900 rad and reconstitution with the indicated bone marrow; mice were allowed to reconstitute for at least 8 weeks prior to use. Mice were housed under specific pathogen-free conditions and used at 8-10 weeks of age, unless otherwise indicated. In all experiments, mice were matched for age and sex before experimental manipulation. All experimental animal procedures were approved by the Institutional Animal Committee of the San Raffaele Scientific Institute.

Infections and immunizations

Unless otherwise indicated, mice were infected intrafootpad with $1x10^5$ plaque-forming units (pfu) of VSV serotype Indiana (Ind), VSV serotype New Jersey (NJ), rVSV (a recombinant VSV expressing a LCMV glycoprotein recognized by both SMARTA TCR transgenic and KL25 BCR transgenic cells instead of the VSV glycoprotein), $1x10^5$ focus forming units (ffu) of LCMV Armstrong (LCMV Arm), LCMV WE, LCMV clone 13 (LCMV Cl13), rLCMV (a recombinant LCMV Clone 13 expressing a LCMV glycoprotein recognized by both SMARTA TCR transgenic and KL25 BCR transgenic cells instead of the LCMV Cl13 glycoprotein)[12,28].

In indicated experiment mice were infected with $1x10^2$, $1x10^5$ or $1x10^7$ pfu of VSV Ind or $1x10^2$, $1x10^5$ or $1x10^7$ ffu of LCMV WE. In indicated experiments mice were infected intravenously with $1x10^6$ ffu of LCMV Arm or LCMV Cl13, or $1x10^6$ pfu of VSV Ind. Viruses were propagated and quantified as described[1228], and diluted in 25 μl of PBS prior to footpad injection or in 200 μl of PBS prior to intravenous injection.

Mice were retro-orbitally bled at the indicated time points for GP-specific Abs measured by GP-1–binding enzyme-linked immunosorbent assay (ELISA)[57]. Anti-mouse IgG1 and IgG2b antibodies of the SBA Clonotyping System-C57BL/6-HRP kit (SouthernBiotech) were used 1:1000 to detect GP-binding Abs.

All infectious work was performed in designated Biosafety Level 2 (BSL-2) and BSL-3 workspaces in accordance with institutional guidelines.

T and B cell isolation, adoptive transfer and in vivo treatments

Naïve $CD4^+$ T cells from spleens of SMARTA $CD45.1^+$, SMARTA GFP^+, SMARTA CFP^+, SMARTA *Ifnar1*$^{-/-}$ transgenic mice, $CD8^+$ T cells from spleens of LCMV-P14-GFP mice and naïve B cells from the spleen of WT mice and KL25-DsRed mice were negatively selected by magnetic isolation (Miltenyi Biotec), with purity always above 98% as determined by flow cytometry. Unless otherwise indicated, 1 x 10^6 SMARTA $CD45.1^+$ T cells were injected intravenously into indicated recipients one day prior to intrafootpad infection. In all imaging experiments, 3 x 10^7 purified naïve B cells were labelled with 1 μM Deep Red (Life Technologies) for 20 min at 37°C in plain RPMI prior to adoptive transfer. In selected imaging experiments (12 hours and 48 hours after infection), 1 x 10^7 or 5 x 10^6 SMARTA GFP^+ or CFP^+, 5 x 10^6 P14 GFP^+, 5 x 10^6 KL25 $DsRed^+$ cells were injected, respectively. In indicated experiments, mice were treated with: the InVivoMab anti-IFNAR (MAR-1 5A3, BioXcell; 1 mg i.v. one day prior to or one day after infection) or mouse IgG1 isotype control (MOPC-21, BioXcell); anti-IL-6 (MP5-20F3, BioXcell; 0.5 mg i.v. one day prior to or one day after infection and 0.25 mg every other day) or rat IgG1 isotype control (BioXcell); the InVivoMab anti-ICOS (7E.17G9, BioXcell, 0.5mg i.v. two and one days prior to infection) or with rat IgG2b isotype control (LTF-2, BioXcell); 25 μg of Poly(I:C) HMW (InvivoGen, intrafootpad injection the day of the infection and one day after). To deplete cDC1 and NK cells, 500 ng of diphtheria toxin (DT, Millipore) diluted in 200 μl of PBS was administered intraperitoneally 1 day before the infection and every other day thereafter to XCR1-DTR and NKp46-DTR mice, respectively.

Cell isolation and flow cytometry

Single-cell suspensions of spleens and LNs were generated as described[28,58]. All flow cytometry stainings of surface-expressed and intracellular molecules were performed as described[28]. Antibodies used included: Bcl-6 (K112-91), T-bet (4B10), CXCR5 (2G8), CD4 (RM4-5), CD45.1 (A20), CD45.2 (K104), CD44 (IM7), IgD (11-26C.2A), NK1.1 (PK136), TCRβ (H57-597), CD8 (K53-6.7), CD11c (N418), CD11b (M1/70), MHCII (AF6-120.1), IgG1 (A85-1) CD95 (JO2), B220 (RA3-6B2), CD69 (H1.2F3) and CD25 (PC61). Fluorochrome-conjugated Abs were purchased from BioLegend, eBioscience or BD Pharmingen. All flow cytometry analyses were performed in FACS buffer containing PBS with 2 mM EDTA and 2% FBS on a FACS CANTO (BD Pharmingen) and analysed with FlowJo software (Treestar).

Confocal immunofluorescence histology

Confocal microscopy analysis of popliteal LNs was performed as previously described[28]. The following primary Abs were used for staining: rat anti-B220 (RA3-6B2), rabbit anti-

GFP (Invitrogen). Images were acquired on an inverted Leica microscope (SP8, Leica Microsystems) with a motorized stage for tiled imaging using a HC PL APO CS2 20X objective (NA 0.75). To minimize fluorophore spectral spill over, we used the Leica sequential laser excitation and detection modality. B cell follicles were defined based on the positioning of polyclonal B cells or by B220 staining. For 3D imaging acquisition, 10 xy stacks (1024 x 1024 pixel) sampled with 2 μm z spacing were acquired to provide image volumes that were 20 μm in depth.

Confocal imaging analysis

Antigen-specific $CD4^+$ T cells were localized using Imaris built-in spot detection function and follicular T cell were identified based on polyclonal B cell positioning. T cell area centre was geometrically identified in Imaris 9.0.2 (Bitplane). Distances from T cell area centre were calculated and normalized for T cell area volumes. A T cell cluster was defined as a minimum of 3 T cells within a distance of 15 μm measured from the centroid of each cell, as previously reported[59]. Spot-to-spot closest distance was calculated to detect ‘clustered’ spots (spot-to-spot closest distance ≤ 15um). Cell clusters of less than 3 cells were manually removed.

Intravital multiphoton microscopy

Mice were anesthetized with 5% isoflurane (Abbot) through a nose cone also delivering oxygen at 1L/min. Follow-up surgery and popliteal LN intravital imaging were carried out with lower concentrations of isoflurane (between 0.5% and 0.8% adjusted based on breathing rate). Surgical preparation of the popliteal LN was performed as described[28,60]. Images were acquired with a LaVision BioTec TriMScope II coupled to an Olympus BX51 up-right microscope enclosed in a custom-built environmental chamber (Life Imaging Services) that was maintained at 37°C with heated air. Continuous body temperature monitoring through a rectal probe was performed to ensure that a narrow range of 37– 38°C was maintained at all times. Fluorescence excitation was provided by two tuneable fs-pulsed Ti:Sa lasers (680–1080 nm, Ultra II, Coherent) and one optical parameter oscillator (1000-1600 nm, APE Chameleon OPO, Coherent). The setup includes four photomultiplier tubes (3 Hamamatsu H7422-40 GaAsP High Sensitivity PMTs and 1 Hamamatsu H7422-50 GaAsP High Sensitivity red- extended PMT) with four emission filters (BS495, ET525/50, ET595/40, BS624) and a high working distance water-immersion 25x objective (NA=1.05, Olympus) or 20x objective (NA=1.0, Zeiss). For 4D analysis of cell migration, stacks of 10 square xy sections (512 x 512 pixel) sampled with 5 μm z spacing were acquired every 10 seconds for up to 1.5 hours to provide image volumes that were 50 μm in depth and with an xy field of view variable between 356 x 356 μm^2 and 409 x 409 μm^2. Sequences of image stacks were transformed into volume-rendered, 4D time-lapse movies with Imaris 9.0.2 (Bitplane). The track speed mean and the meandering index (the ratio of a migrating cell’s linear displacement to the total path length) were calculated by semi-automated cell tracking algorithm of Imaris.

Intravital cytometry

Intravital cytometry was performed by adapting a method for histocytometry[61]. Briefly, T cell and B cell surfaces were created by the surface object creation wizard in Imaris 9.0.2

(Bitplane). T and B cell surfaces were then merged into T-B surfaces using the merge function in Imaris. Channel statistics from T-B-merged surfaces were exported and merged into combined CSV files (Python) that were uploaded and analysed on FlowJo X[61].

Niche-seq

Niche-seq was performed as previously described[18]. Briefly, Olympus BX51 upright microscope fitted with tuneable fs-pulsed Ti:Sa lasers was used to photoactivate and image niches of interest (680–1080 nm, Ultra II, Coherent). Images were acquired with a two-photon laser tuned to 940 nm. Regions within the outer paracortex of draining LNs (with Ag-specific $CD4^+$ T cell clusters) were photoactivated at 820 nm[19]. Tile images were acquired as a 20-30 μm Z-stacks with 5 μm steps between each Z-plane. Images were acquired at 512 x 512 x-y resolution. The volume and depth along the Z axis of the photoactivated zones were consistent among experiments.

Immediately after photoactivation, lymph nodes were forced through a 70 μm mesh into ice cold FACS buffer (EDTA pH8.0 2mM, BSA 0,5% in PBS). Cell populations were sorted with BD FACSAria fusion (BD Biosciences). Because in individual photoactivated cells only a fraction of the inactive-PA-GFP is converted to active-PA-GFP, photoactivated PA-GFP cells express both the activated PA-GFP (detectable upon 488 nm excitation) as well as the inactive PA-GFP (detectable upon 405 nm excitation) by flow cytometry. After doublets exclusion, isolated cells were single-cell sorted into 384-well cell capture plates containing 2 μL of lysis solution and barcoded poly(T) reverse-transcription (RT) primers for single-cell RNA-seq. Four empty wells were kept in each 384-well plate as a no-cell control during data analysis. Immediately after sorting, each plate was spun down to ensure cell immersion into the lysis solution, snap frozen on dry ice, and stored at –80°C until processed.

Single-cell RNA-seq

Dendritic cells were sorted with BD FACSAria fusion (BD Biosciences). After doublets exclusion, cells positive for CD11c and MHC-II but negative for CD3 and B220 were single-cell sorted into 384-well cell capture plates containing 2 μL of lysis solution and barcoded poly(T) reverse-transcription (RT) primers for single-cell RNA-seq. Immediately after sorting, each plate was spun down to ensure cell immersion into the lysis solution, snap frozen on dry ice, and stored at –80°C until processed.

Massively Parallel Single-Cell RNA-seq library preparation (MARS-seq)

Single-cell libraries were prepared as previously described[62]. Briefly, mRNA from cell sorted into cell capture plates were barcoded and converted into cDNA and pooled using an automated pipeline. The pooled sample was then linearly amplified by T7 in vitro transcription, and the resulting RNA was fragmented and converted into a sequencing-ready library by tagging the samples with pool barcodes and Illumina sequences during ligation, RT, and PCR. Each pool of cells was tested for library quality and concentration was assessed as described[62].

All RNA-Seq libraries (pooled at equimolar concentration) were sequenced using Illumina NextSeq 500 at a median sequencing depth of 38,323 reads per cell. Sequences were

mapped to mouse genome (mm9), demultiplexed, and filtered as described[62], extracting a set of unique molecular identifiers (UMI) that define distinct transcripts in single cells for further processing. We estimated the level of spurious UMIs in the data using statistics on empty MARS-seq wells and excluded all plates with estimated noise > 5%. Mapping of reads was done using HISAT (version 0.1.6); reads with multiple mapping positions were excluded. Reads were associated with genes if they were mapped to an exon, using the UCSC genome browser for reference. Exons of different genes that shared genomic position on the same strand were considered a single gene with a concatenated gene symbol. Cells with less than 500 UMIs were discarded from the analysis.

Clustering of infected lymph nodes

For clustering of scRNA-seq of infected lymph nodes we used the R package MetaCell[36]. MetaCell was used to derive informative genes and compute cell-to-cell similarity, to compute K-nn graph covers and derive distribution of RNA in cohesive groups of cells (or meta-cells), and to derive strongly separated clusters using bootstrap analysis and computation of graph covers on resampled data. Default parameters were used unless otherwise stated. Cells from rVSV- and rLCMV-infected lymph nodes were clustered together. Meta-cells were annotated by pooled differential expression of marker genes, using the $FP_{gene,mc}$ metric, which signifies for each gene and meta-cell the fold change between the geometric mean of this gene within the meta-cell and the median geometric mean across all meta-cells. Each gene was given a FP threshold and a priority index – such that colouring for Activated T cells by *Gzma* is favoured over colouring for general T cells by *Trbc2*. The selected genes, priority, and fold change threshold parameters are as follows:

group	gene	priority	fold change
T	*Trbc2*	1	2
T	*Cd3e*	1	2
CD8T	*Cd8a*	2	2.5
NK	*Klrb1c*	3	2
actT	*Gzma*	4	2
unknown	*Gm23935*	3	2
CD4T	*Cd4*	3	1.5
DC	*Cxcl16*	5	2
Mono	*Fcer1g*	2	3
B	*Cd79b*	3	0.6

Clustering of dendritic cells

For clustering of scRNA-seq of $CD11c^{+}$ MHC-II^{high} DCs, we used the R package MetaCell[36], as previously described. Cells from rVSV- and rLCMV-infected lymph nodes, from all time points and genetic backgrounds were clustered together. Meta-cells were annotated by pooled differential expression of marker genes, as described before. The selected genes, priority, and fold change threshold parameters are as follows:

group	gene	priority	fold change
Migratory cDC2	Fscn1	1	5
Migratory cDC2	Il12b	1	2
cDC1	Naaa	1	3
cDC1	Cd24a	1	2.5
cDC2	Cd209a	2	5
cDC2	Cd209d	2	1.8
Mo-DC	Csf1r	4	3
Mo-DC	Tgfbi	4	2
Mo-DC	Fcer1g	4	2
Macrophages	C1qb	5	4

qPCR

Total RNA was isolated from frozen LNs with ReliaPrep RNA Miniprep system (Promega), following the manufacturer's instructions. 1 μg of total RNA was reverse transcribed prior to qPCR analyses for *Ifna2* (Mm00833961_S1, Thermo Fisher), *Ifna4* (Mm00833969_S1, Thermo Fisher), *Ifna5* (Mm00833976_S1, Thermo Fisher), *Ifna6* (Mm01703458_S1, Thermo Fisher), *Ifna7* (Mm02525960_S1, Thermo Fisher), *Ifna9* (Mm00833983_S1, Thermo Fisher), *Ifna12* (Mm00616656_S1, Thermo Fisher), *Ifna13* (Mm01731013_S1, Thermo Fisher), *Ifna14* (Mm01703465_S1, Thermo Fisher), *Ifnb* (Mm00439552_S1, Thermo Fisher), *Isg15* (Mm 01705338_S1,hermo Fisher), *2'5'Oas* (Mm00460961_m1, Thermo Fisher) and *IL-6* (Mm00446190_M1, Thermo Fisher) in a QuantStudio 5 Real-Time PCR System (Thermo Fisher Scientific). All experiments were done in duplicate and normalized to the housekeeping gene *GAPDH* (Mm99999915_g1, Thermo Fisher).

Statistical analyses

Results are expressed as mean ± SEM. All statistical analyses were performed in Prism 5 (GraphPad Software). Means between two groups were compared with unpaired two-tailed t test. Means among three or more groups were compared with one-way or two-way ANOVA. Bonferroni post-test was used to correct for multiple comparisons, and in some experiments the Fisher's Least Significant Difference (LSD) post-test was used when correction for multiple comparisons was not necessary.

Extended Data

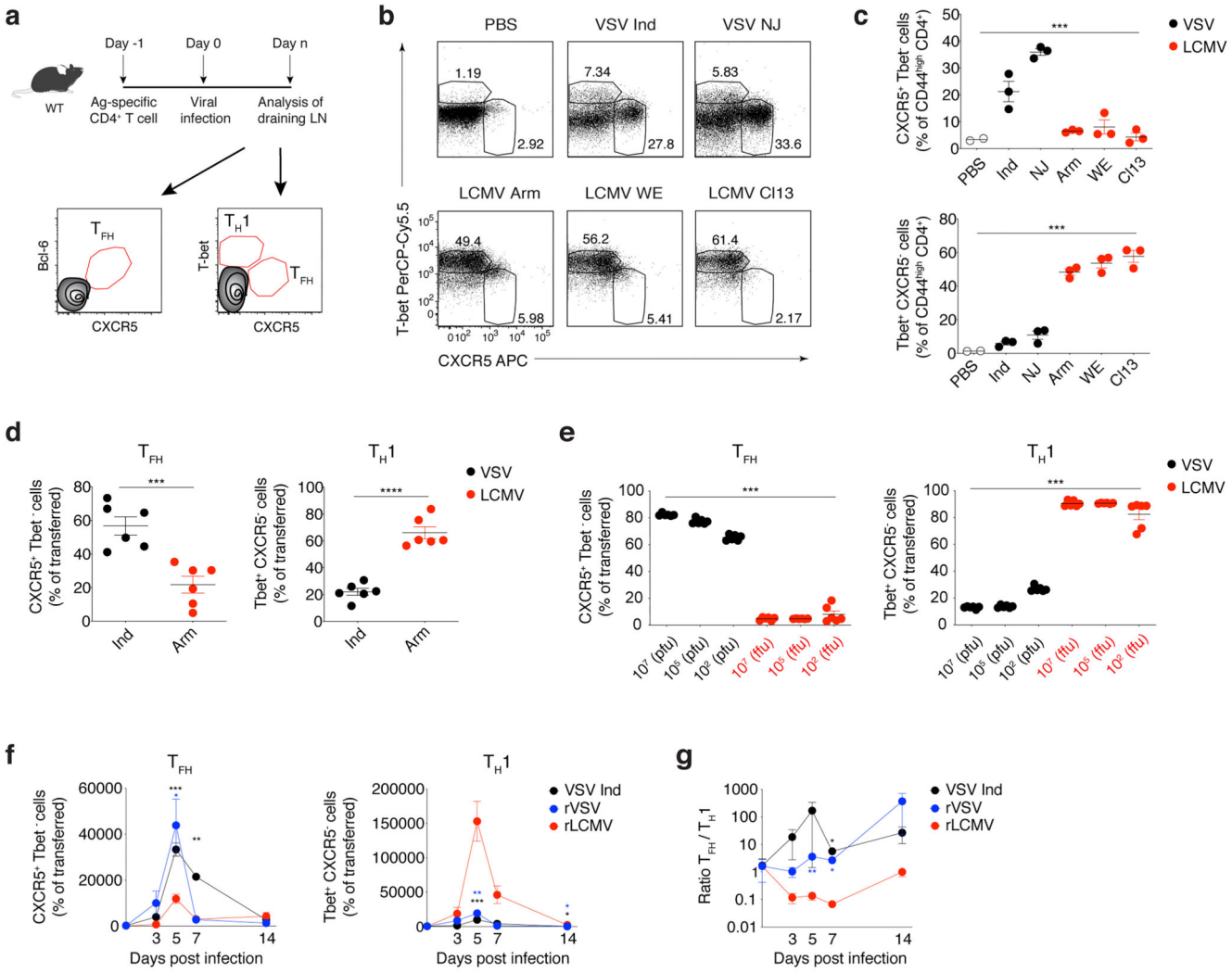

Extended Data Fig. 1. VSV and LCMV infections result in distinct antiviral CD4$^+$ T cell polarization and in vivo dynamic behavior, independently of viral strain, viral dose, infection route and TCR signal strength.

(**a**) Schematic representation of experimental procedure for the results described in Fig. 1a-c. 1 x 10^6 purified Ag-specific (Tg7 when VSV-Ind was used, SMARTA cells in all other cases) CD45.1$^+$ CD4$^+$ T cells were injected into CD45.2$^+$ WT recipients 1 day before intrafootpad infection. dLNs were collected at the indicated time points after infection and analyzed by flow cytometry. T_{FH} were defined as either Bcl-6$^+$ CXCR5$^+$ or CXCR5$^+$ T-bet$^-$ cells (in the latter case we always verified that cells were also Bcl-6$^+$); T_H1 were defined as T-bet$^+$ CXCR5$^-$ cells. (**b**) Representative flow cytometry plots showing T_{FH} and T_H1 cells (out of CD44^{high} endogenous CD4$^+$ T cells) in dLNs 7 days after footpad infection with the indicated virus. Numbers indicated the percentage of cells within the indicated gate. Results are representative of at least 2 independent experiments. (**c**) Quantification of T_{FH} (top) and T_H1 cells (bottom) – expressed as percentages of CD44^{high} endogenous CD4$^+$ T cells – in dLNs of mice described in **b.** Results are representative of at least 2 independent experiments. Mean+/- SEM is shown. PBS *n*=2, all other conditions n=3. A one-way Anova

Europe PMC Funders Author Manuscripts

test was applied; *** *p value < 0.001*. (**d**) Quantification of T_{FH} (left) and T_H1 (right) cells (expressed as percentages out of total transferred cells) in the spleens of CD45.2$^+$ WT recipients injected with 1 x 10^6 Ag-specific (Tg7 when VSV-Ind was used, SMARTA in all other cases) CD45.1$^+$ T cells one day prior to intravenous infection with VSV-Ind (left), LCMV-Arm (right) or LCMV-Cl13 (not shown), respectively. Mean+/- SEM is shown. An unpaired two-tailed t test was applied. *** *p value < 0.001.* (**e**) Quantification of T_{FH} (left) and T_H1 (right) cells (expressed as percentages out of total transferred cells) in dLNs 5 days after infection of CD45.2$^+$ WT recipients injected with 1 x 10^6 Ag-specific (Tg7 for VSV-Ind, SMARTA for LCMV-WE) CD45.1$^+$ T cells one day prior to intrafootpad infection with the indicated doses of VSV-Ind (black) or LCMV-WE (red). Results are pooled from 2 independent experiments. Mean+/- SEM is shown.*n*=6. A one-way Anova test was applied. *** *p value < 0.001.* (**f-g**) Quantification of T_{FH} (left) and T_H1 (right) cell absolute numbers (**f**) or T_{FH}/T_H1 absolute number ratios (**g**) at 0,3,5,7 and 14 days after VSV-Ind (black), rVSV (blue) or rLCMV (red) infection. Mean+/- SEM is shown. Day 0 *n* = 3 (VSV), 4 (rVSV and rLCMV); Day 3 *n* = 5 (VSV), 7 (rVSV and rLCMV); Day 5 *n* = 5 (VSV), 9 (rVSV), 10 (rLCMV); Day 7 *n* = 3; Day 14 *n* = 3 (VSV and rVSV), 6 (rLCMV). Black and blue stars indicate significance of respectively VSV and rVSV samples towards LCMV samples. A two-way Anova with LSD post-test was applied. ** p value < 0.05; ** p value < 0.01; *** p value < 0.001; **** p value < 0.0001*.

Europe PMC Funders Author Manuscripts

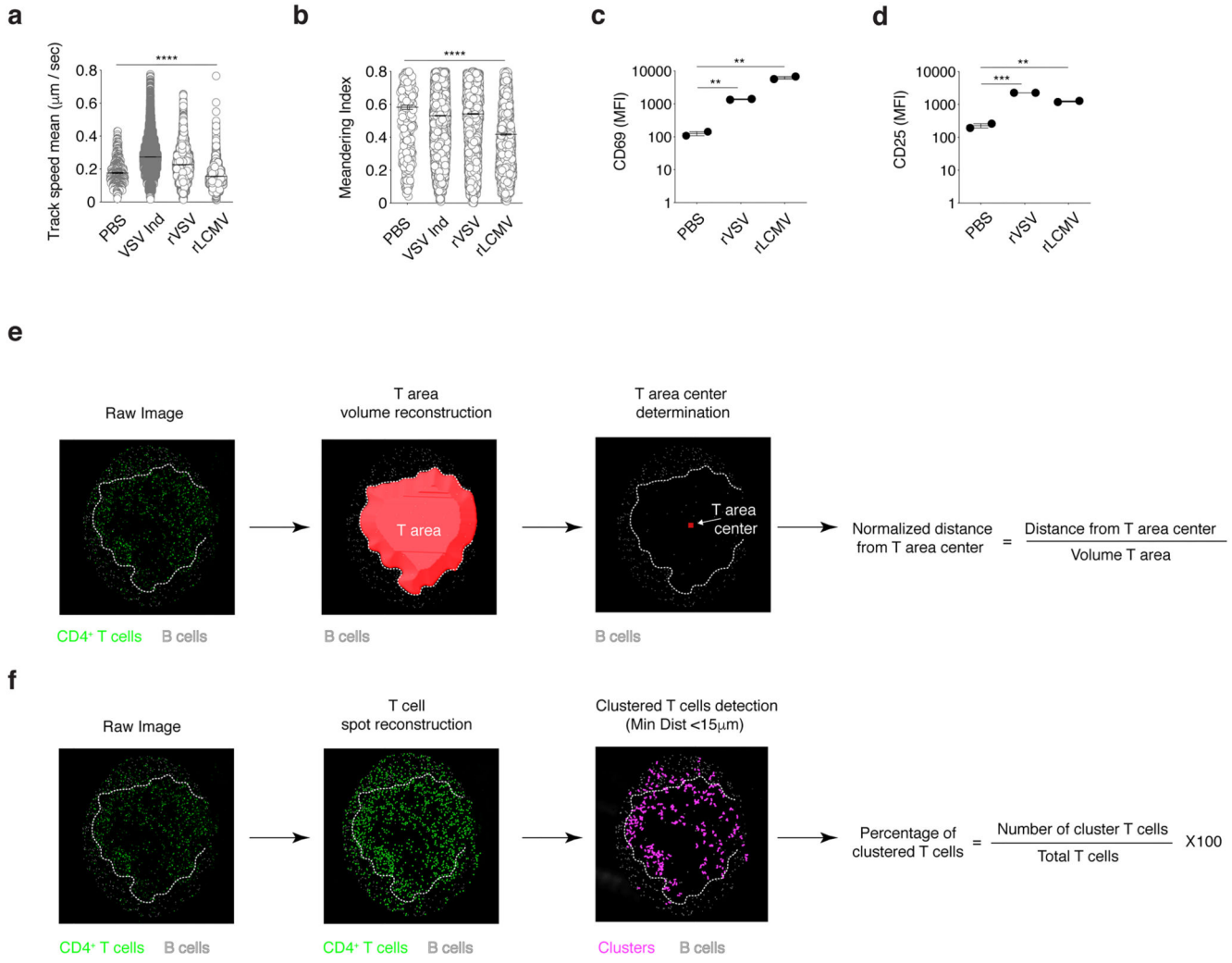

Extended Data Fig. 2. Spatiotemporal dynamics and activation of Ag-specific CD4$^+$ T cells within dLNs upon VSV or LCMV infection.

(**a, b**) Track speed mean (**a**) and meandering index (**b**) of GFP$^+$ Ag-specific (Tg7 when VSV-Ind was used, SMARTA in all other cases) CD4$^+$ T cells in the mice described in Fig. 1d-g and Supplementary Movie 1, 3 days after PBS, VSV-Ind, rVSV or rLCMV injection. Data are pooled from 2 independent experiments. PBS, *n*=395; VSV-Ind *n*=11219; rVSV *n=6692;* rLCMV *n*=3537. One-way Anova test was applied. **** *p value < 0.0001;* (**c, d**) Mean fluorescent intensity of CD69 (**c**) and CD25 (**d**) within Ag-specific (SMARTA) CD4$^+$ T cells in dLNs, 2 days after PBS, rVSV or rLCMV injection. Data are representative of 2 independent experiments. Mean+/- SEM is shown. *n*=2. One-way Anova test was applied. *** p value < 0.01;* *** *p value < 0.001* (**e, f**) Methods used to determine the normalized distance from T area centre (**e**) and percentages of clustered T cells / section (**f**). (**e**) T cell area volume was defined based on polyclonal B cell positioning and its centre was geometrically identified in Imaris. Ag-specific CD4$^+$ T cells were localized using Imaris built-in spot detection function and distance from T cell area centre was calculated and normalized for T cell are volumes. (**f**) A T cell cluster was defined as a minimum of 3 T

Europe PMC Funders Author Manuscripts

cells aggregating within closest distance of 15 μm measured from cell centroids (see Materials and Methods). Cell clusters of less than 3 cells were manually removed.

Europe PMC Funders Author Manuscripts

Europe PMC Funders Author Manuscripts

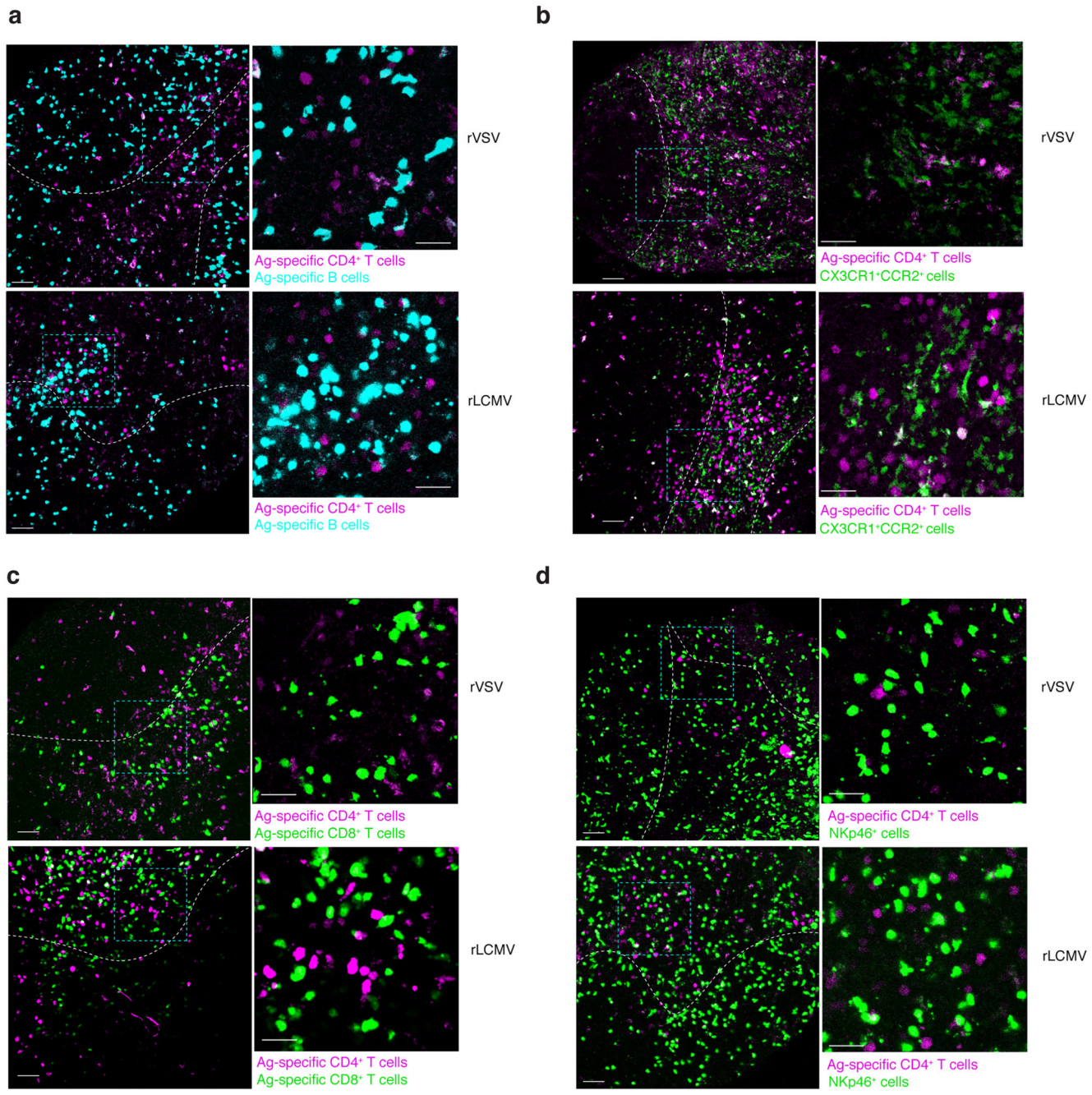

Extended Data Fig. 3. Confocal analysis of the CD4$^+$ T cell priming niche.

Confocal imaging of murine dLNs collected 2 days after rVSV or rLCMV infection. Dashed lines represent the edges of B cell follicles and were depicted based on B220 staining. (**a**) Ag-specific GFP$^+$ CD4$^+$ T cells (SMARTA, depicted in purple) and Ag-specific CFP$^+$ B cells (KL25, depicted in cyan) were adoptively transferred into WT mice. (**b**) Ag-specific CFP$^+$ CD4$^+$ T cells (SMARTA, depicted in purple) were adoptively transferred into CX3CR1-GFP x CCR2-RFP mice. A colocalization channel for GFP and RFP was used to depict inflammatory monocytes (cells positive for both CX3CR1 and CCR2, in green). (**c**)

Ag-specific CFP^+ $CD4^+$ T cells (SMARTA, depicted in purple) and Ag-specific GFP^+ $CD8^+$ T cells (P14, depicted in green) were adoptively transferred into WT mice. (**d**) Ag-specific CFP^+ $CD4^+$ T cells (SMARTA, depicted in purple) were adoptively transferred into NKp46-ZsGreen mice. Scale bars represent 50 μm or 30 μm (zoom). The dotted square represents the zoomed area in the IFA where $CD4^+$ T cell clusters are found. All images are representative of at least 2 independent experiments.

Europe PMC Funders Author Manuscripts

Europe PMC Funders Author Manuscripts

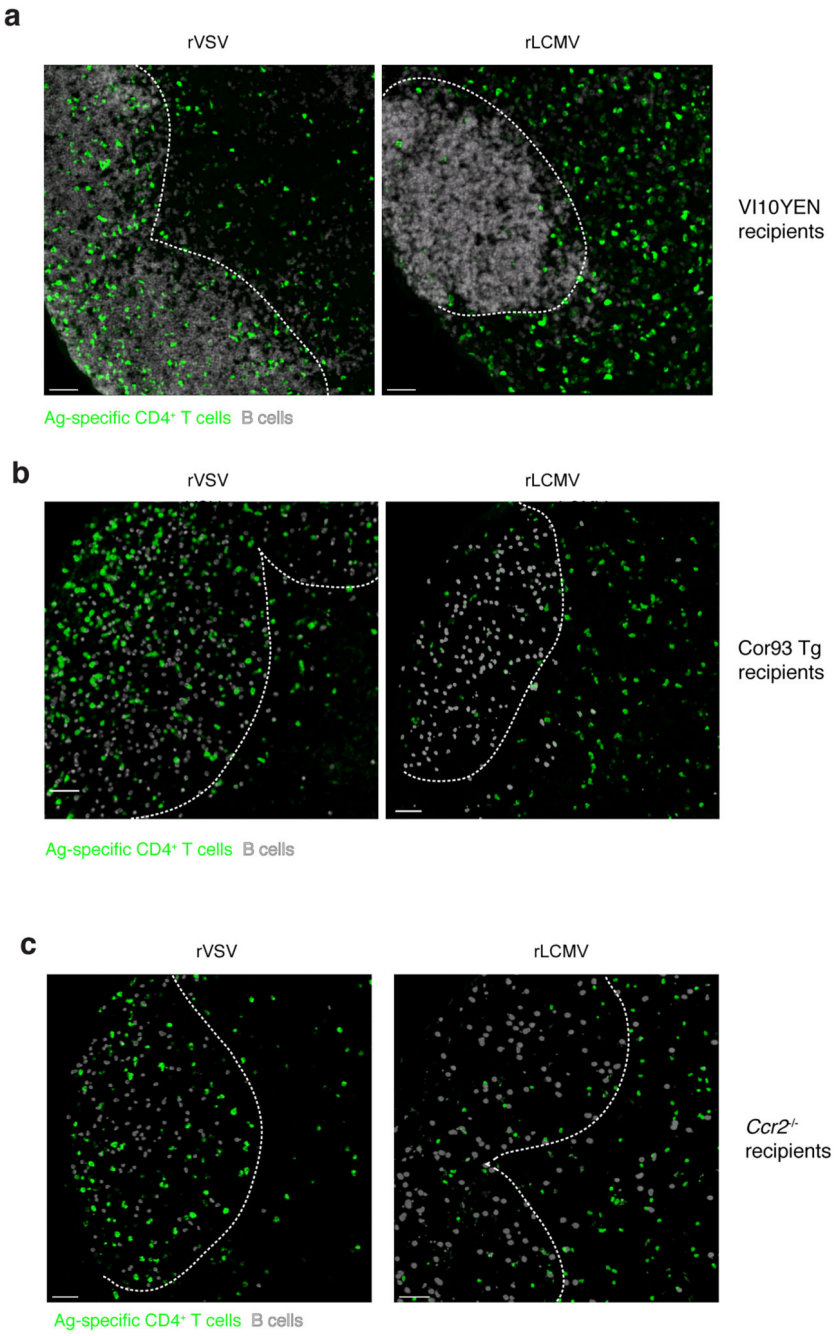

Extended Data Fig. 4. Early antiviral CD4$^+$ T cell localization is independent of Ag-specific B cells, Ag-specific CD8$^+$ T cells and CCR2+ monocytes.

Confocal imaging of dLNs of VI10YEN (**a**), Cor93 Tg TCR (**b**), and CCR2$^{-/-}$ (**c**) mice collected either 3 (**a**) or 5 (**b, c**) days after rVSV (*left*) or rLCMV (*right*) infection. Ag-specific CD4$^+$ T cells are depicted in green. Dashed lines represent the edges of B cell follicles and were depicted based on polyclonal B cell positioning (**b, c**) or B220 staining (**a**) (both in grey). Scale bars represent 50 μm. Results are representative of at least 2 independent experiments.

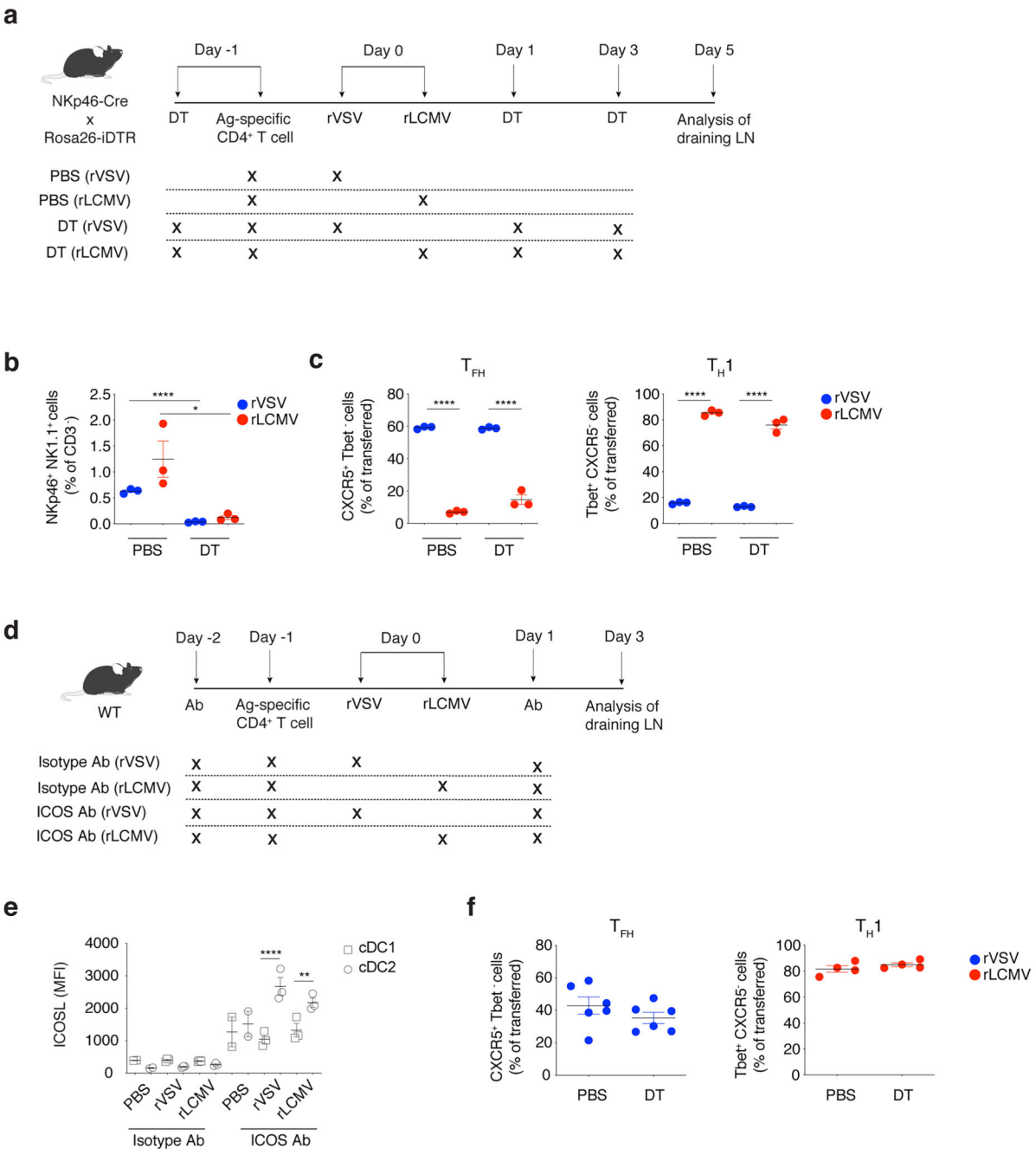

Extended Data Fig. 5. Antiviral CD4$^+$ T cell are primed by cDC2 cells and differentiate independently of NK cells.

(**a**) Schematic representation of the experimental procedure for the results described in panels **b** and **c**. 1 x 10^6 purified CD45.1$^+$ Ag-specific (SMARTA) CD4$^+$ T cells were injected into NKp46-DTR mice treated with PBS or DT as indicated. dLNs were collected 5 days after rVSV (blue) or rLCMV (red) infection. Percentages of NK cells (**b**), T_{FH} (**c**, *left*) and T_H1 (**c**, *right*) in dLNs were quantified by flow cytometry. Data are representative of 2 independent experiments. Mean+/- SEM is shown. *n*=3. A one-way Anova with

Europe PMC Funders Author Manuscripts

Europe PMC Funders Author Manuscripts

Bonferroni's post-test was applied. ** p value < 0.05; **** p value < 0.0001* (**d**) Schematics of the experimental setup for the results described in panel **e**. 1 x 10^6 purified CD45.1$^+$ Ag-specific (SMARTA) CD4$^+$ T cells were transferred to WT mice treated with anti-ICOS blocking antibody or with isotype control, as indicated, prior to rVSV (blue) or rLCMV (red) infection. dLNs were collected 3 days after infection. (**e**) ICOSL expression (mean fluorescent intensity) within CD11c$^+$ MHC-II^{high} CD8$^+$ (cDC1) and CD11c$^+$ MHC-II^{high} CD11b$^+$ (cDC2) cell subsets in dLNs of the mice described in **d**. Data are representative of 2 independent experiments. Mean+/- SEM is shown. PBS conditions *n*=2, all other conditions *n=3*. A one-way Anova with Bonferroni's post-test was applied. *** p value < 0.01; **** p value < 0.0001.* (**f**) 1 x 10^6 purified CD45.1$^+$ Ag-specific (SMARTA) CD4$^+$ T cells were transferred to WT and DT-treated XCR1-DTR mice prior to rVSV (blue, *left*) or rLCMV (red, *right*) infection. Quantification of T_{FH} (*left*) and T_H1 (*right*) – expressed as percentages of the total transferred cells – in dLNs 5 days after infection is shown. Mean+/- SEM is shown. Data are representative of 2 independent experiments. *n*=4-6.

Europe PMC Funders Author Manuscripts

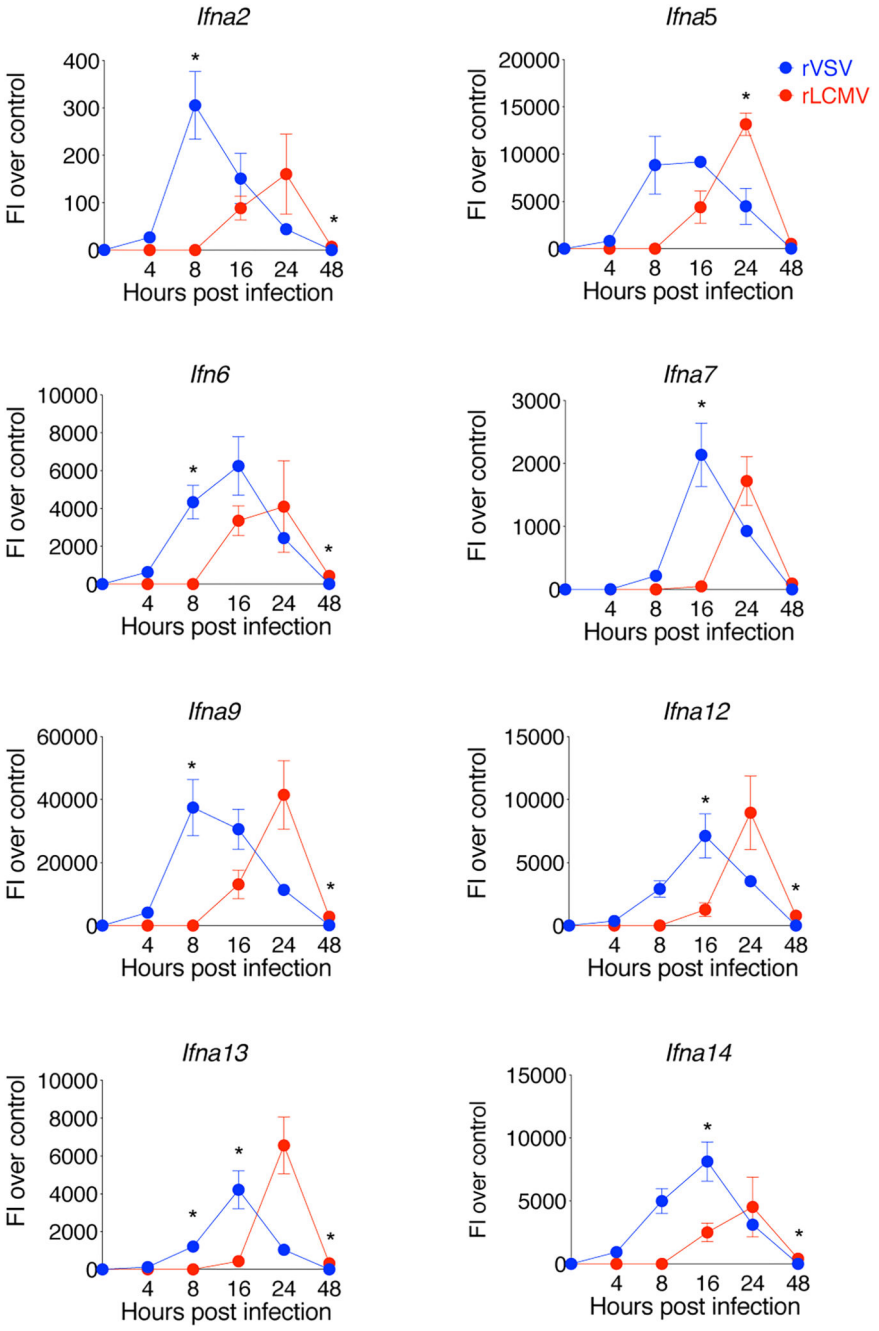

Extended Data Fig. 6. Measurement of IFN-α isoforms upon rVSV and rLCMV infection.

Analysis of *Ifna2*, *Ifna5, Ifna6, Ifna7, Ifna9, Ifna12, Ifna13, Ifna14* gene expression in dLN at 0, 4, 8, 16, 24 and 48 hours after rVSV (blue) or rLCMV (red) infection by qPCR. Data are pooled from 2 independent experiments. Mean+/- SEM is shown. 0 hours $n = 3$; 4 hours $n = 4$; 8 hours $n = 3$ (rLCMV), 4 (rVSV); 16 hours $n = 3$ (rLCMV), 4 (rVSV); 24 hours $n = 2$ (rLCMV), 4 (rVSV); 48 hours $n = 4$. A two-way Anova with LSD post-test was applied. * *p value* < 0.05. The same sample was measured repeatedly for the 4 genes.

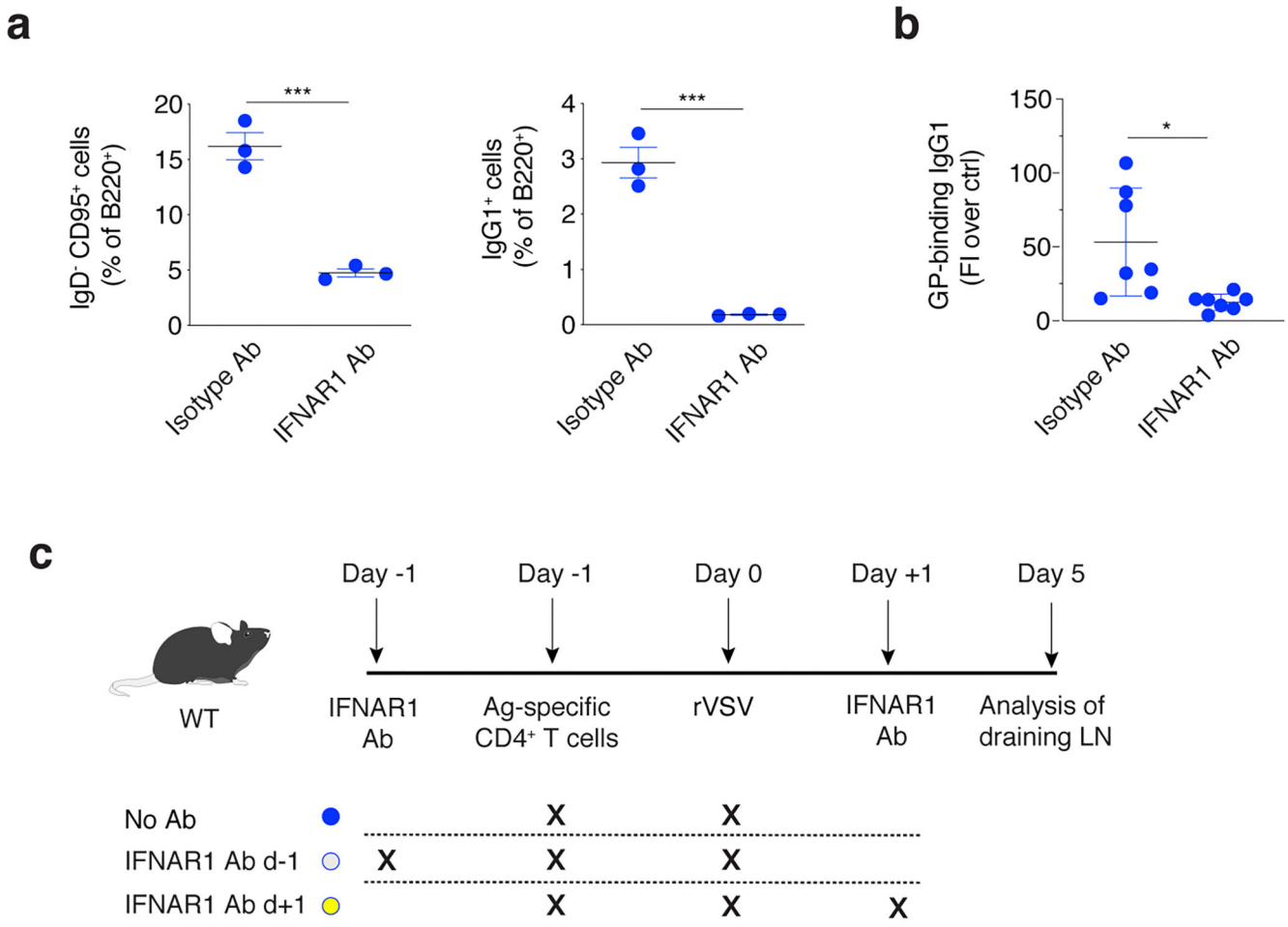

Extended Data Fig. 7. Early type I IFN signalling promotes germinal centre B cells and antiviral antibody responses

a) Quantification of IgD^{-} CD95^{+} germinal centre (GC) B cells (left) – expressed as percentage of B220^{+} cells – and of IgG1^{+} cells (right) – expressed as percentage of B220^{+} B cells – in the dLNs of mice treated with anti-IFNAR blocking antibody (or isotype control), and infected with rVSV 14 days earlier. Mean+/- SEM is shown. *n=3*. An unpaired two-tailed t test was applied. *** *p value < 0.001.* (**b**) GP–binding IgG1 Abs (expressed as fold induction over uninfected controls) were measured in the sera of mice described in panel A, 14 days after rVSV infection. Data are pooled from 2 independent experiments. Mean+/- SEM is shown. *n*=7. An unpaired two-tailed t test was applied. ** p value < 0.05.* (**c**) Schematic representation of experimental procedure for the results described in Fig 3d-f. 1 x 10^{6} purified CD45.1^{+} Ag-specific (SMARTA) CD4^{+} T cells were transferred to CD45.2^{+} WT recipients and treated anti-IFNAR1 blocking antibody either 1 day prior to (light blue) or 1 day after (yellow) rVSV infection.

Europe PMC Funders Author Manuscripts

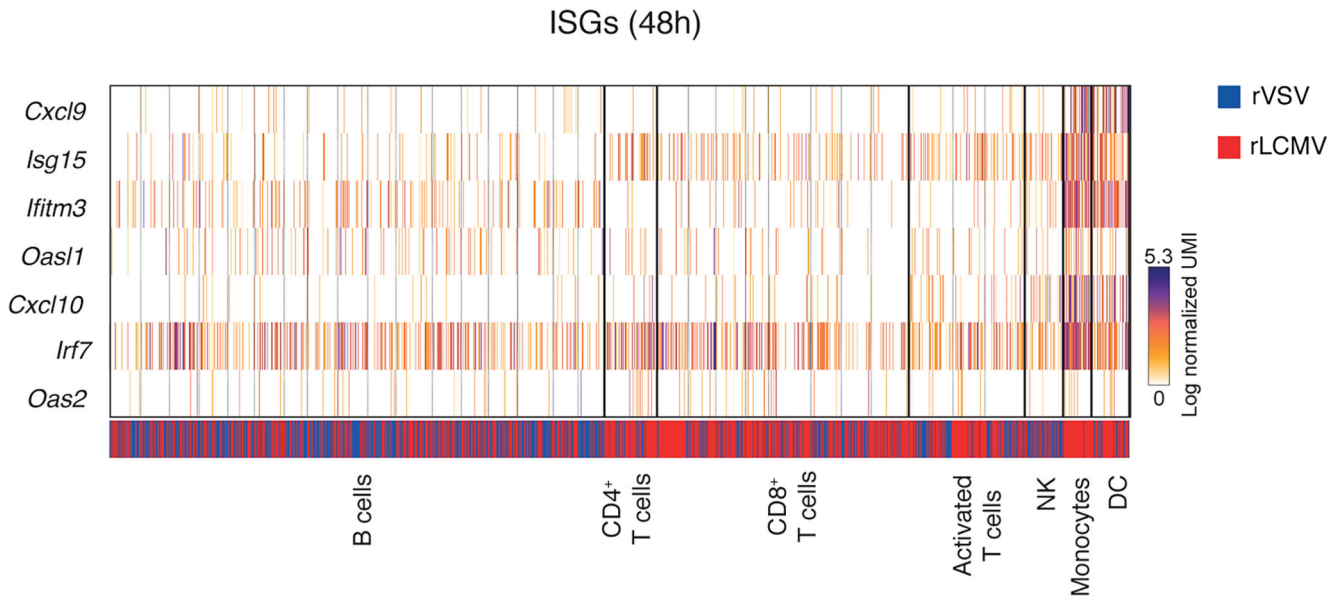

Extended Data Fig. 8. Expression of interferon stimulated genes within the cellular components of the CD4$^+$ T cell priming niche.

Expression of the indicated interferon-stimulated genes (ISGs) within the cellular components of the photoactivated CD4$^+$ T cell priming niches of the mice described in Fig. 2d-f. The colour bar on the bottom indicates each cell's origin (blue: photoactivated cells from rVSV; red: photoactivated cells from rLCMV).

Europe PMC Funders Author Manuscripts

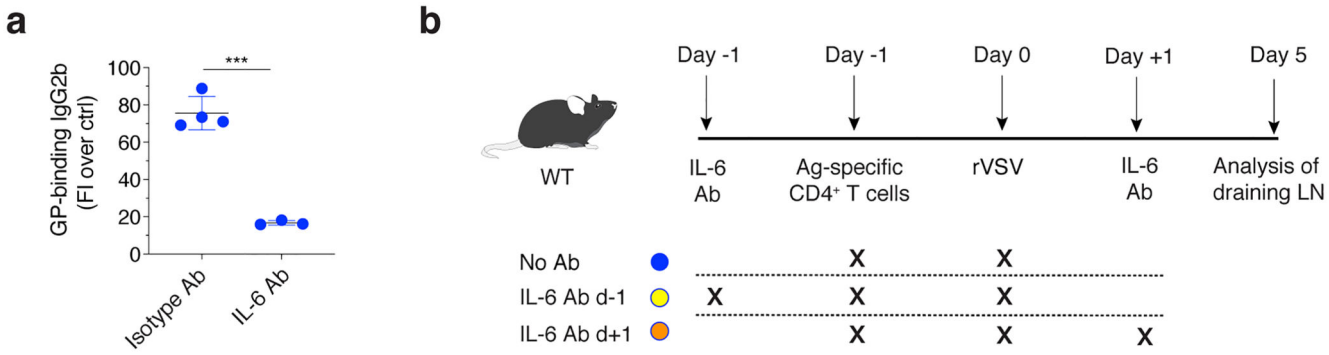

Extended Data Fig. 9. Blocking IL-6 impairs antiviral antibody responses.

(**a**) WT mice were treated with anti-IL-6 blocking antibody (or isotype control) and sera were collected 14 days after rVSV infection. GP–binding IgG2b Abs were measured in the sera and expressed as fold induction over uninfected controls. Data are representative of 2 independent experiments. Mean+/- SEM is shown. An unpaired two-tailed t test was applied. *** *p value < 0.001.* (**b**) Schematic representation of experimental procedure for the results described in Fig. 4e. 1 x 10^6 purified CD45.1$^+$ Ag-specific (SMARTA) CD4$^+$ T cells were transferred to CD45.2$^+$ WT recipients and treated with anti-IL-6 blocking antibody starting either 1 day prior to (yellow) or 1 day after rVSV infection (orange).

Europe PMC Funders Author Manuscripts

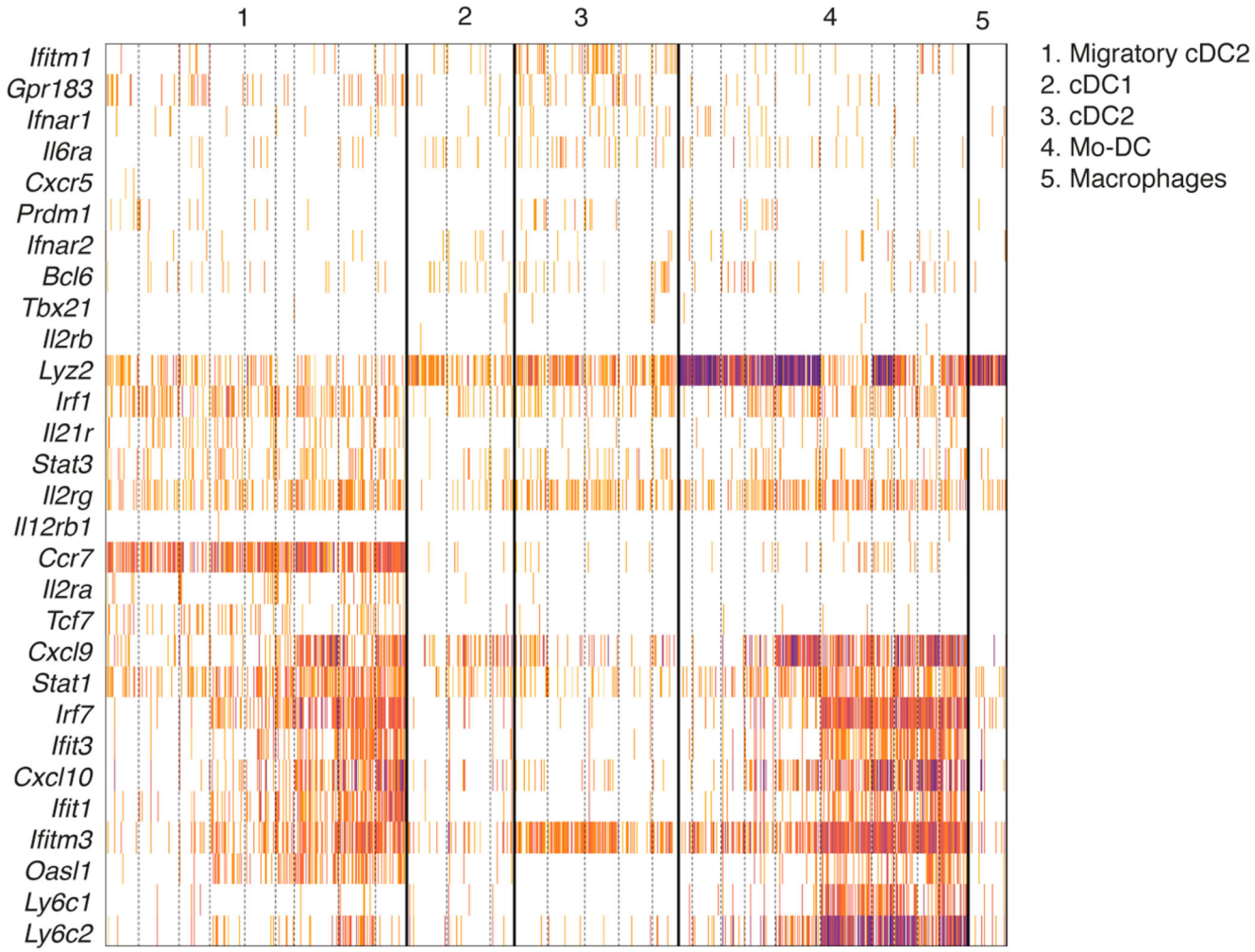

Extended Data Fig. 10. Expression of interferon stimulated genes in dendritic cells.

Expression of different ISGs across 2179 single QC positive CD11c^{+} MHC-II^{high} cells grouped in 5 clusters as described in the legend to Fig. 5A.

Supplementary Material

Refer to Web version on PubMed Central for supplementary material.

Acknowledgments

We thank M. Mainetti and M. Freschi for technical support; M. Silva for secretarial assistance; J.C. de la Torre for providing rLCMV; D. Pinschewer for providing rVSV; M. Linterman for providing Cd11-Cre x *Ifnar1*$^{fl/fl}$ bone marrow; R. Pardi and A. Mondino for critical reading of the manuscript and the members of the Iannacone laboratory for helpful discussions. Confocal immunofluorescence histology was carried out at Alembic, San Raffaele Scientific Institute and the Vita-Salute San Raffaele University. Flow cytometry was carried out at FRACTAL, San Raffaele Scientific Institute. We would like to acknowledge the PhD program in Basic and Applied Immunology and Oncology at Vita-Salute San Raffaele University, as V.C. and E.S. conducted this study as partial fulfilment of their PhD in Molecular Medicine within that program. M.I. is supported by European Research Council (ERC) Consolidator Grant 725038, Italian Association for Cancer Research (AIRC) Grants 19891 and 22737, Italian Ministry of Health (MoH) Grant GR-2011-02347925, Lombardy Foundation for Biomedical Research (FRRB) Grant 2015-0010, the European Molecular Biology Organization Young Investigator Program,

and a Career Development from the Giovanni Armenise-Harvard Foundation; M.K. is supported by the Italian Ministry of Education grants SIR-RBSI14BAO5 and PRIN-2017ZXT5WR.

References

1. Hale JS, et al. Distinct memory CD4+ T cells with commitment to T follicular helper- and T helper 1-cell lineages are generated after acute viral infection. Immunity. 2013; 38:805–817. [PubMed: 23583644]
2. Wu T, et al. Cutting Edge: miR-17-92 Is Required for Both CD4 Th1 and T Follicular Helper Cell Responses during Viral Infection. J Immunol. 2015
3. Crotty S. Follicular Helper CD4 T Cells (T). Annu Rev Immunol. 2011; 29:621–663. [PubMed: 21314428]
4. Vinuesa CG, Linterman MA, Yu D, MacLennan IC. Follicular Helper T Cells. Annu Rev Immunol. 2016; 34:335–368. [PubMed: 26907215]
5. Szabo SJ, et al. A novel transcription factor, T-bet, directs Th1 lineage commitment. Cell. 2000; 100:655–669. [PubMed: 10761931]
6. Arnaout RA, Nowak MA. Competitive coexistence in antiviral immunity. J Theor Biol. 2000; 204:431–441. [PubMed: 10816366]
7. Hangartner L, Zinkernagel RM, Hengartner H. Antiviral antibody responses: the two extremes of a wide spectrum. Nat Rev Immunol. 2006; 6:231–243. [PubMed: 16498452]
8. Kuka M, Iannacone M. Viral subversion of B cell responses within secondary lymphoid organs. Nat Rev Immunol. 2018; 18:255–265. [PubMed: 29249807]
9. Maloy KJ, et al. Qualitative and quantitative requirements for CD4+ T cell-mediated antiviral protection. J Immunol. 1999; 162:2867–2874. [PubMed: 10072535]
10. Oxenius A, Bachmann MF, Zinkernagel RM, Hengartner H. Virus-specific MHC-class II-restricted TCR-transgenic mice: effects on humoral and cellular immune responses after viral infection. Eur J Immunol. 1998; 28:390–400. [PubMed: 9485218]
11. Fazilleau N, McHeyzer-Williams LJ, Rosen H, McHeyzer-Williams MG. The function of follicular helper T cells is regulated by the strength of T cell antigen receptor binding. Nat Immunol. 2009; 10:375–384. [PubMed: 19252493]
12. Fallet B, et al. Interferon-driven deletion of antiviral B cells at the onset of chronic infection. Sci Immunol. 2016; 1
13. Osokine I, et al. Type I interferon suppresses de novo virus-specific CD4 Th1 immunity during an established persistent viral infection. Proc Natl Acad Sci U S A. 2014; 111:7409–7414. [PubMed: 24799699]
14. Kerfoot SM, et al. Germinal center B cell and T follicular helper cell development initiates in the interfollicular zone. Immunity. 2011; 34:947–960. [PubMed: 21636295]
15. Mempel TR, Henrickson SE, Von Andrian UH. T-cell priming by dendritic cells in lymph nodes occurs in three distinct phases. Nature. 2004; 427:154–159. [PubMed: 14712275]
16. Gerner MY, Casey KA, Kastenmuller W, Germain RN. Dendritic cell and antigen dispersal landscapes regulate T cell immunity. J Exp Med. 2017; 214:3105–3122. [PubMed: 28847868]
17. Groom JR, et al. CXCR3 chemokine receptor-ligand interactions in the lymph node optimize CD4+ T helper 1 cell differentiation. Immunity. 2012; 37:1091–1103. [PubMed: 23123063]
18. Medaglia C, et al. Spatial reconstruction of immune niches by combining photoactivatable reporters and scRNA-seq. Science. 2017; 358:1622–1626. [PubMed: 29217582]
19. Victora GD, et al. Germinal center dynamics revealed by multiphoton microscopy with a photoactivatable fluorescent reporter. Cell. 2010; 143:592–605. [PubMed: 21074050]
20. Hangartner L, et al. Antiviral immune responses in gene-targeted mice expressing the immunoglobulin heavy chain of virus-neutralizing antibodies. Proc Natl Acad Sci U S A. 2003; 100:12883–12888. [PubMed: 14569006]
21. Cook KD, Kline HC, Whitmire JK. NK cells inhibit humoral immunity by reducing the abundance of CD4+ T follicular helper cells during a chronic virus infection. J Leukoc Biol. 2015; 98:153–162. [PubMed: 25986014]

Europe PMC Funders Author Manuscripts

22. Narni-Mancinelli E, et al. Fate mapping analysis of lymphoid cells expressing the NKp46 cell surface receptor. Proc Natl Acad Sci U S A. 2011; 108:18324–18329. [PubMed: 22021440]
23. Buch T, et al. A Cre-inducible diphtheria toxin receptor mediates cell lineage ablation after toxin administration. Nat Methods. 2005; 2:419–426. [PubMed: 15908920]
24. Odermatt B, Eppler M, Leist TP, Hengartner H, Zinkernagel RM. Virus-triggered acquired immunodeficiency by cytotoxic T-cell-dependent destruction of antigen-presenting cells and lymph follicle structure. Proc Natl Acad Sci U S A. 1991; 88:8252–8256. [PubMed: 1910175]
25. Borrow P, Evans CF, Oldstone MB. Virus-induced immunosuppression: immune system-mediated destruction of virus-infected dendritic cells results in generalized immune suppression. J Virol. 1995; 69:1059–1070. [PubMed: 7815484]
26. Moseman EA, Wu T, de la Torre JC, Schwartzberg PL, McGavern DB. Type I interferon suppresses virus-specific B cell responses by modulating CD8+ T cell differentiation. Sci Immunol. 2016; 1
27. Isogawa M, Chung J, Murata Y, Kakimi K, Chisari FV. CD40 activation rescues antiviral $CD8^+$ T cells from PD-1-mediated exhaustion. PLoS Pathog. 2013; 9:e1003490. [PubMed: 23853599]
28. Sammicheli S, et al. Inflammatory monocytes hinder antiviral B cell responses. Sci Immunol. 2016; 1
29. Boring L, et al. Impaired monocyte migration and reduced type 1 (Th1) cytokine responses in C-C chemokine receptor 2 knockout mice. J Clin Invest. 1997; 100:2552–2561. [PubMed: 9366570]
30. Eisenbarth SC. Dendritic cell subsets in T cell programming: location dictates function. Nat Rev Immunol. 2018
31. Li J, Lu E, Yi T, Cyster JG. EBI2 augments Tfh cell fate by promoting interaction with IL-2-quenching dendritic cells. Nature. 2016; 533:110–114. [PubMed: 27147029]
32. Kuka M, De Giovanni M, Iannacone M. The role of type I interferons in CD4+ T cell differentiation. Immunol Lett. 2019
33. Nurieva RI, et al. Generation of T follicular helper cells is mediated by interleukin-21 but independent of T helper 1, 2, or 17 cell lineages. Immunity. 2008; 29:138–149. [PubMed: 18599325]
34. Eto D, et al. IL-21 and IL-6 are critical for different aspects of B cell immunity and redundantly induce optimal follicular helper CD4 T cell (Tfh) differentiation. PLoS One. 2011; 6:e17739. [PubMed: 21423809]
35. Cucak H, Yrlid U, Reizis B, Kalinke U, Johansson-Lindbom B. Type I interferon signalling in dendritic cells stimulates the development of lymph-node-resident T follicular helper cells. Immunity. 2009; 31:491–501. [PubMed: 19733096]
36. Baran Y, Sebe-Pedros A, Lubling Y, BioRxiv AG. MetaCell: analysis of single cell RNA-seq data using k-NN graph partitions. biorxiv.org. 2018
37. Chakarov S, Fazilleau N. Monocyte-derived dendritic cells promote T follicular helper cell differentiation. EMBO Mol Med. 2014; 6:590–603. [PubMed: 24737871]
38. Scheu S, Dresing P, Locksley RM. Visualization of IFNbeta production by plasmacytoid versus conventional dendritic cells under specific stimulation conditions in vivo. Proc Natl Acad Sci U S A. 2008; 105:20416–20421. [PubMed: 19088190]
39. Kumagai Y, et al. Alveolar macrophages are the primary interferon-alpha producer in pulmonary infection with RNA viruses. Immunity. 2007; 27:240–252. [PubMed: 17723216]
40. Iannacone M, et al. Subcapsular sinus macrophages prevent CNS invasion on peripheral infection with a neurotropic virus. Nature. 2010; 465:1079–1083. [PubMed: 20577213]
41. Trinchieri G. Lymphocyte choriomeningitis virus plays hide-and-seek with type 1 interferon. Cell Host Microbe. 2012; 11:553–555. [PubMed: 22704613]
42. Gaya M, et al. Host response. Inflammation-induced disruption of SCS macrophages impairs B cell responses to secondary infection. Science. 2015; 347:667–672. [PubMed: 25657250]
43. Kawano Y, Noma T, Kou K, Yoshizawa I, Yata J. Regulation of human IgG subclass production by cytokines: human IgG subclass production enhanced differentially by interleukin-6. Immunology. 1995; 84:278–284. [PubMed: 7751005]

44. Hsieh CS, et al. Development of TH1 CD4+ T cells through IL-12 produced by Listeria-induced macrophages. Science. 1993; 260:547–549. [PubMed: 8097338]
45. Bradley LM, Dalton DK, Croft M. A direct role for IFN-gamma in regulation of Th1 cell development. J Immunol. 1996; 157:1350–1358. [PubMed: 8759714]
46. Heufler C, et al. Interleukin-12 is produced by dendritic cells and mediates T helper 1 development as well as interferon-gamma production by T helper 1 cells. Eur J Immunol. 1996; 26:659–668. [PubMed: 8605935]
47. Oxenius A, Karrer U, Zinkernagel RM, Hengartner H. IL-12 is not required for induction of type 1 cytokine responses in viral infections. J Immunol. 1999; 162:965–973. [PubMed: 9916721]
48. Schijns VE, et al. Mice lacking IL-12 develop polarized Th1 cells during viral infection. J Immunol. 1998; 160:3958–3964. [PubMed: 9558103]
49. Madisen L, et al. A robust and high-throughput Cre reporting and characterization system for the whole mouse brain. Nat Neurosci. 2010; 13:133–140. [PubMed: 20023653]
50. Pircher H, Bürki K, Lang R, Hengartner H, Zinkernagel RM. Tolerance induction in double specific T-cell receptor transgenic mice varies with antigen. Nature. 1989; 342:559–561. [PubMed: 2573841]
51. Müller U, et al. Functional role of type I and type II interferons in antiviral defense. Science. 1994; 264:1918–1921. [PubMed: 8009221]
52. Yamazaki C, et al. Critical roles of a dendritic cell subset expressing a chemokine receptor, XCR1. J Immunol. 2013; 190:6071–6082. [PubMed: 23670193]
53. Caton ML, Smith-Raska MR, Reizis B. Notch-RBP-J signalling controls the homeostasis of CD8- dendritic cells in the spleen. J Exp Med. 2007; 204:1653–1664. [PubMed: 17591855]
54. Prigge JR, et al. Type I IFNs Act upon Hematopoietic Progenitors To Protect and Maintain Hematopoiesis during Pneumocystis Lung Infection in Mice. J Immunol. 2015; 195:5347–5357. [PubMed: 26519535]
55. Jung S, et al. Analysis of fractalkine receptor CX(3)CR1 function by targeted deletion and green fluorescent protein reporter gene insertion. Mol Cell Biol. 2000; 20:4106–4114. [PubMed: 10805752]
56. Saederup N, et al. Selective chemokine receptor usage by central nervous system myeloid cells in CCR2-red fluorescent protein knock-in mice. PLoS One. 2010; 5:e13693. [PubMed: 21060874]
57. Eschli B, et al. Early antibodies specific for the neutralizing epitope on the receptor binding subunit of the lymphocytic choriomeningitis virus glycoprotein fail to neutralize the virus. J Virol. 2007; 81:11650–11657. [PubMed: 17699567]
58. Tonti E, et al. Bisphosphonates target B cells to enhance humoral immune responses. Cell Rep. 2013; 5:323–330. [PubMed: 24120862]
59. Hor JL, et al. Spatiotemporally Distinct Interactions with Dendritic Cell Subsets Facilitates CD4+ and CD8+ T Cell Activation to Localized Viral Infection. Immunity. 2015; 43:554–565. [PubMed: 26297566]
60. Sammicheli S, Kuka M, Iannacone M. Intravital Imaging of B Cell Responses in Lymph Nodes. Methods Mol Biol. 2018; 1763:63–74. [PubMed: 29476489]
61. Tan Y, et al. Streamlining volumetric multi-channel image cytometry using hue-saturation-brightness-based surface creation. Commun Biol. 2018; 1:136. [PubMed: 30272015]
62. Jaitin DA, et al. Massively parallel single-cell RNA-seq for marker-free decomposition of tissues into cell types. Science. 2014; 343:776–779. [PubMed: 24531970]

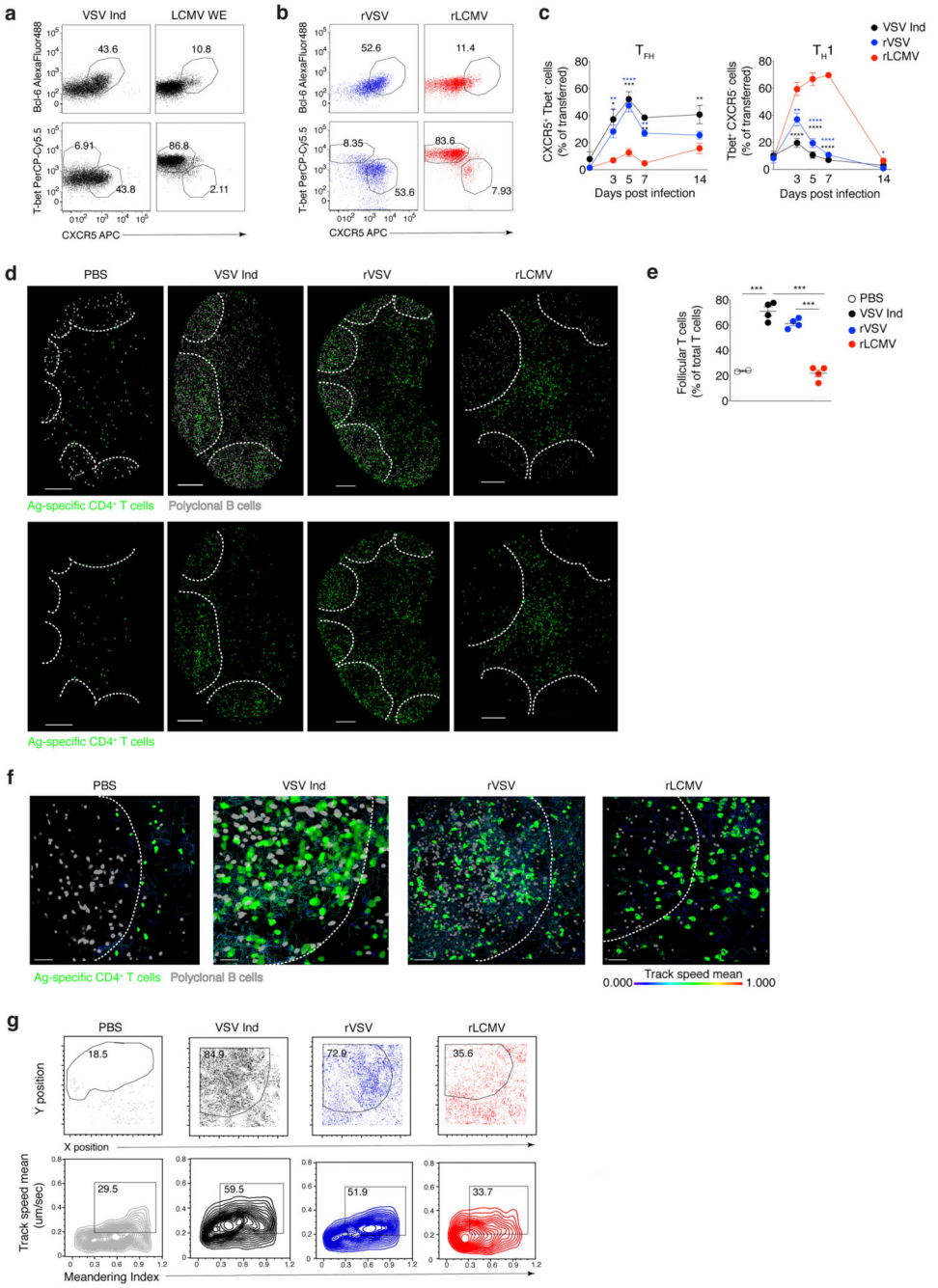

Fig. 1. VSV and LCMV infections result in distinct antiviral CD4$^+$ T cell polarization and in vivo dynamics

(**a**) Representative flow cytometry plots of transferred CD45.1$^+$ Tg7 CD4$^+$ T cells or CD45.1$^+$ SMARTA CD4$^+$ T cells (1 x 10^6 each) in the footpad-draining popliteal LNs (dLNs) of CD45.2$^+$ wild-type recipient mice 5 days post intrafootpad infection with VSV Ind (left) or LCMV WE (right), respectively (Extended Data 1a for schematic representation of experimental set up). Numbers indicate percentages within the indicated gates. Plots are representative of at least 5 independent experiments. (**b**) Representative flow cytometry plots

of transferred CD45.1$^+$ SMARTA CD4$^+$ T cells (1 x 10^6) in the footpad-draining popliteal LNs (dLNs) of CD45.2$^+$ wild-type recipient mice 5 days post intrafootpad infection with rVSV (left) or rLCMV (right). Numbers indicate percentages within the indicated gates. Plots are representative of at least 5 independent experiments. (**c**) Quantification of T_{FH} cells (left) or T_H1 cells (right) as percentages of the transferred Tg7 (in case of VSV Ind infection) or SMARTA (in case of infection with rVSV or rLCMV) CD45.1$^+$ CD4$^+$ T cells in dLNs of CD45.2$^+$ wild-type recipients at 0, 3, 5, 7 and 14 days post-infection. Mean+/- SEM is shown. Day 0 n = 3 (VSV), 4 (rVSV and rLCMV); day 3 n = 5 (VSV), 7 (rVSV and rLCMV); day 5 n = 5 (VSV), 9 (rVSV), 10 (rLCMV); day 7 n = 3; day 14 n = 3 (VSV and rVSV), 6 (rLCMV). Black and blue stars indicate significance of VSV and rVSV samples, respectively, compared to rLCMV samples. A two-way Anova with LSD post-test was applied. ** $p < 0.05$; ** $p < 0.01$; *** $p < 0.001$; **** $p < 0.0001$* (**d**) Confocal micrographs of dLNs in wild-type (WT) mice injected with 1 x 10^6 purified GFP$^+$ Tg7 (VSV Ind) or SMARTA (all other groups) CD4$^+$ T cells (green) and 3 x 10^7 purified deep red-labelled polyclonal B cells (grey), 1 day prior to injection with PBS, VSV Ind, rVSV and rLCMV. The images on the bottom are the same as the images on top except that the channel pertaining to polyclonal B cells was removed to improve clarity. Images were collected 3 days after infection and are representative of at least 3 independent experiments. Scale bars represent 200 μm. (**e**) Quantification of follicular Ag-specific CD4$^+$ T cells in dLNs of mice as in **d**. Mean+/- SEM is shown. n=2 (PBS), 4 (VSV Ind, rVSV, rLCMV). A one-way Anova with Bonferroni's post-test was applied. *** *$p < 0.001$* (**f**) Snapshots from multiphoton intravital imaging of dLNs in WT mice injected with 1 x 10^6 purified GFP$^+$ Tg7 (VSV Ind) or SMARTA (all other groups) CD4$^+$ T cells (green) and 3 x 10^7 purified deep red-labelled polyclonal B cells (grey), injected 1 day prior to injection with PBS, VSV Ind, rVSV and rLCMV (see Supplementary Movie 1). Cell tracks are coloured based on track speed mean values (blue = 0 μm/sec; red =1 μm/sec; see Supplementary Movie 1). Dashed lines define B cell follicles and were depicted based on polyclonal B cell positioning. Data are representative of at least 2 independent experiments. (**g**) Intravital cytometry plots of the movies in **g** showing either Tg7 (VSV Ind) or SMARTA (all other groups) CD4$^+$ T cell XY cell positions over time (top), or meandering index versus track speed mean (bottom, see Supplementary Movie 1). Gates represent percentages of follicular CD4$^+$ T cell tracks (top) and meandering index^{hi}track speed mean^{hi} CD4$^+$ T cell tracks (bottom). Numbers indicate the percentage of tracks within the indicated gates. Data are representative of at least 2 independent experiments.

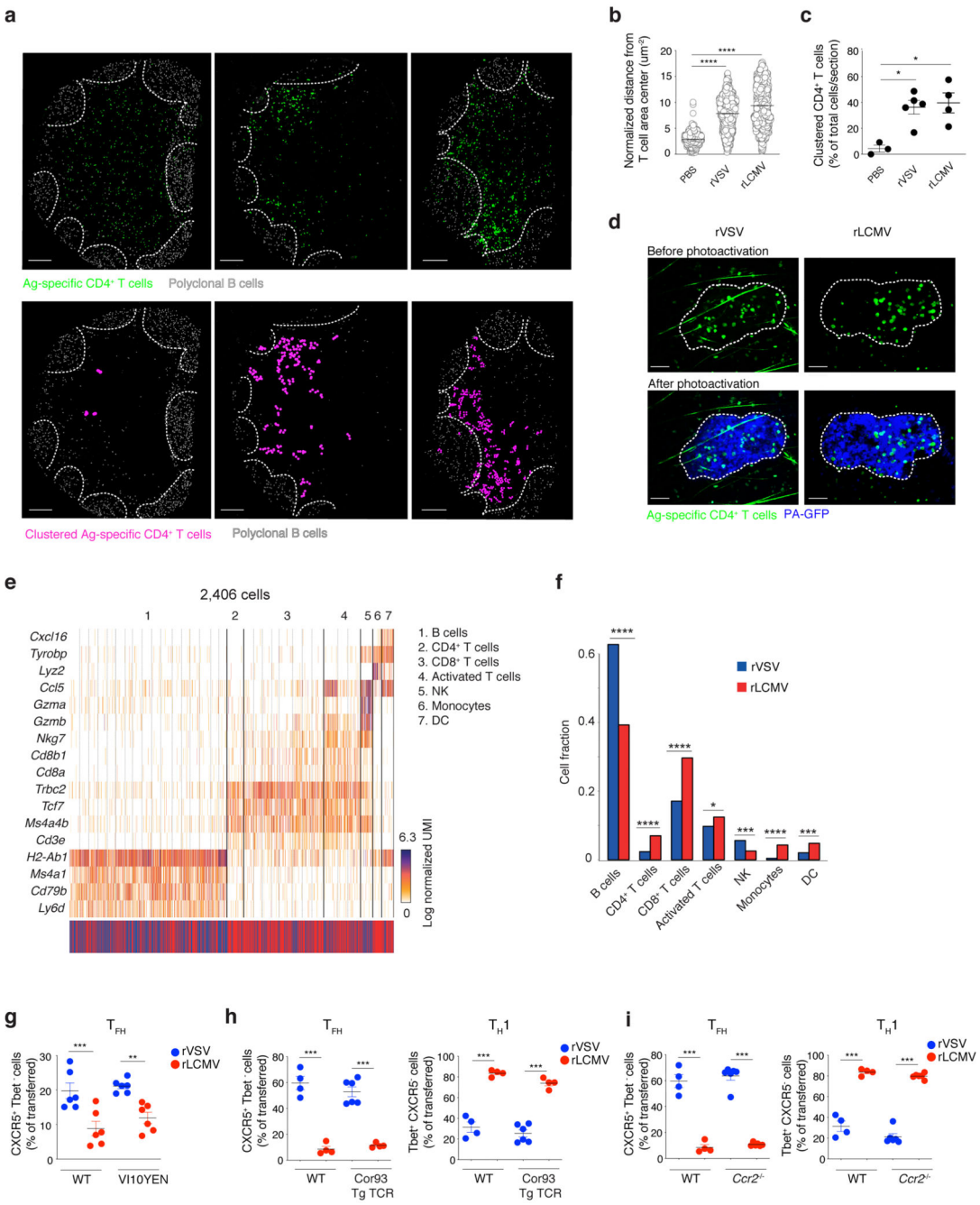

Fig. 2. Characterization of the antiviral CD4$^+$ T cell priming niche.

(**a**) Confocal micrographs of dLNs in mice injected with 5 x 10^6 purified GFP$^+$ Ag-specific (SMARTA) CD4$^+$ T cells (green) and 3 x 10^7 purified deep red-labelled polyclonal B cells (grey), 1 day before injection with PBS, rVSV or rLCMV. Images were acquired 2 days after infection and are representative of at least 2 independent experiments. The top panels depict the positioning of GFP$^+$ Ag-specific (SMARTA) T cells whereas the bottom panels indicate the clustered Ag-specific (SMARTA) T cells (purple). A T cell cluster was defined as a minimum of 3 T cells within a distance of 15 μm measured from the centroid of each cell

Europe PMC Funders Author Manuscripts

Europe PMC Funders Author Manuscripts

(see Materials and Methods). Scale bars represent 200 μm. See also Supplementary Movie 2. (**b, c**) Quantification of the normalized distance of Ag-specific (SMARTA) T cells from the T cell area centre (**b**) and percentages of clustered T cells / section (**c**) in the mice described in **a**. Mean+/- SEM is shown. PBS *n* =772, rVSV *n*=1025, rLCMV *n*=1127 (**b**); PBS *n* = 3, rVSV *n*=5, rLCMV *n*=4 (**c**). Results are pooled from 2 independent experiments. A one-way Anova with Bonferroni's post-test was applied. * $p < 0.05$; **** $p < 0.0001$. (**d**) Multiphoton intravital micrographs depicting the photoactivation of the $CD4^+$ T cell priming niche upon rVSV or rLCMV infection. Images were acquired 2 days after infection. Ag-specific (SMARTA) CFP^+ $CD4^+$ T cells are depicted in green and PA-GFP^+ in blue. Top panels, before photoactivation; bottom panels, after photoactivation. Scale bars represent 50 μm. Images are representative of at least 2 independent experiments. (**e**) Gene expression profiles of 2406 single cells from photoactivated priming niches, grouped in 7 clusters. The colour bar on the bottom indicates each cell's origin (blue: photoactivated cells from rVSV infected mice; red: photoactivated cells from rLCMV infected mice). (**f**) Relative abundance of different cell clusters within $CD4^+$ T cell priming niches. Data represent cell counts from two biological replicates. Two-sided FDR-adjusted Fisher's exact test. * $p < 0.05$; *** $p < 0.001$; **** $p < 0.0001$. (**g-i**) 1 x 10^6 purified $CD45.1^+$ Ag-specific (SMARTA) $CD4^+$ T cells were injected into $CD45.2^+$ WT recipients and into either VI10YEN (**g,** *n=6*), Cor93 Tg TCR (**h,** *n=4 or 6*), or *Ccr2*$^{-/-}$ (**I,** *n=4 or 6*) mice. dLNs were collected 3 (**g**) or 5 (**h-i**) days after rVSV (blue) or rLCMV (red) infection. Percentages of T_{FH} (**g-i**, *left*) and T_H1 (**h-i**, *right*) Ag-specific $CD4^+$ T cells out of total transferred cells in dLNs were quantified by flow cytometry. Data are representative of at least 2 independent experiments. Mean+/- SEM is shown. A one-way Anova with Bonferroni's post-test was applied. ** $p < 0.01$; *** $p < 0.001$

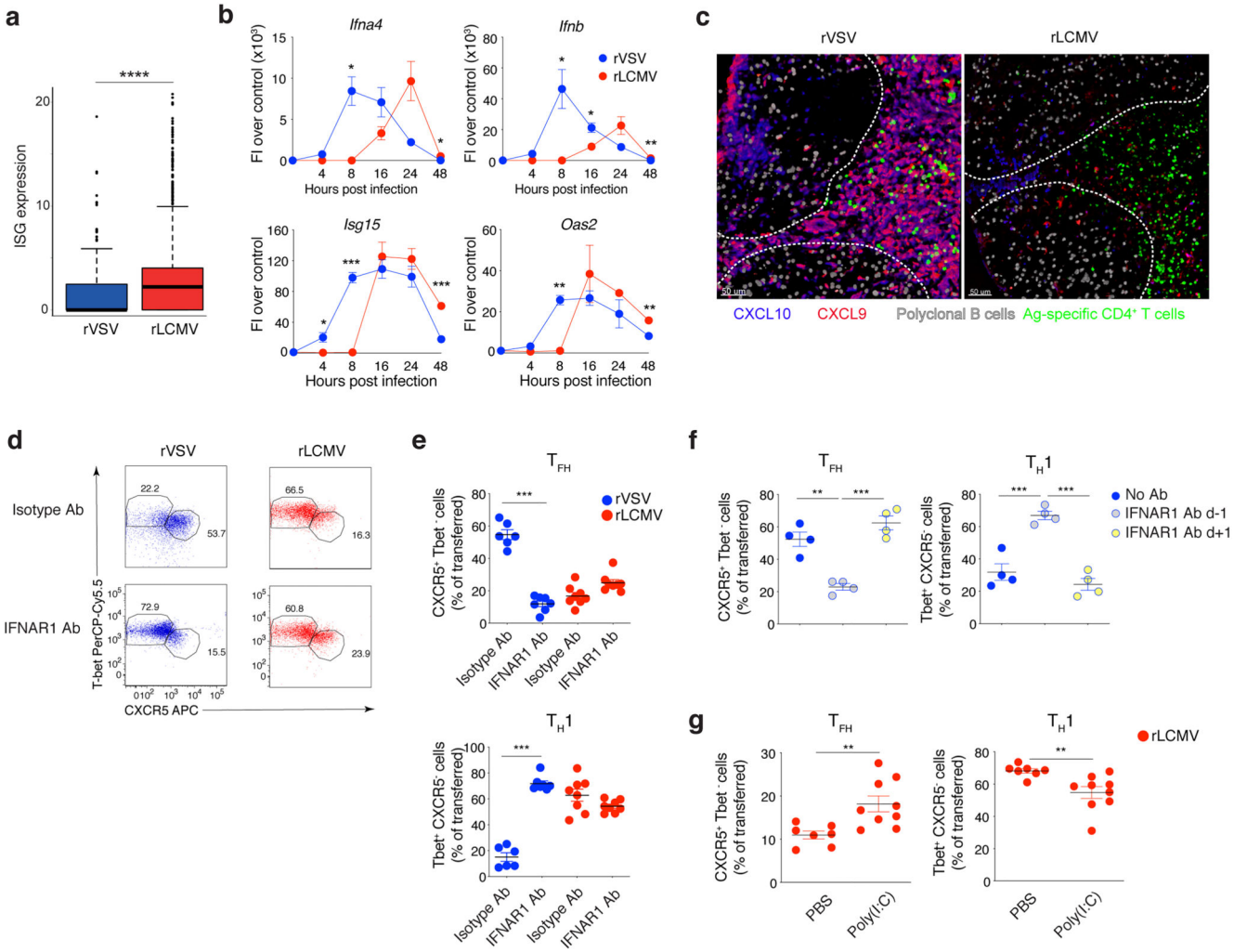

Fig. 3. Spatiotemporal regulation of type I IFN expression determines antiviral CD4$^+$ T cell polarization.

(**a**) Expression profile of selected ISGs (*Irf7*, *Cxcl9*, *Cxcl10*, *Oasl1*, *Ifitm3*, *Oas2*, *Isg15*) in 2406 single cells from the photoactivated CD4$^+$ T cell priming niches described in Fig. 2 d-f. Data are pooled from 2 independent experiments. Kolmogorov–Smirnov test was applied. **** $p < 0.0001$. (**b**) Analysis of *Ifna4*, *Ifnb* (*top*) and *Isg15*, *Oas2* (*bottom*) gene expression in dLN at 0, 4, 8, 16, 24 and 48 hours after rVSV (blue) or rLCMV (red) infection by qPCR. 0 hours $n = 3$; 4 hours $n = 4$; 8 hours $n = 4$; 16 hours $n = 4$; 24 hours $n = 3$ (rLCMV), 4 (rVSV); 48 hours $n = 4$. Data are pooled from 2 independent experiments. Mean+/- SEM is shown. A two-way Anova with LSD post-test was applied. * $p < 0.05$; ** $p < 0.01$; *** $p < 0.001$. The same sample was measured repeatedly for the 4 genes. (**c**) Confocal micrographs of dLNs in REX3 reporter mice injected with 1 x 10^7 purified GFP$^+$ Ag-specific (SMARTA) CD4$^+$ T cells (green) and 3 x 10^7 purified deep-labelled polyclonal B cells (grey), 12 hours after rVSV or rLCMV infection. CXCL10$^+$ (blue) and CXCL9$^+$ (red) cells are depicted. Data are representative of at least 2 independent experiments. (**d**) Representative flow cytometry plots show T_{FH} and T_H1 within Ag-specific CD4$^+$ T cells, 5 days after infection of CD45.2$^+$ WT recipients injected with 1 x 10^6 purified CD45.1$^+$ SMARTA CD4$^+$ T cells

and treated with anti-IFNAR1 blocking antibody (or isotype control) 1 day prior to rVSV (blue, *left*) or rLCMV (red, *right*) infection. Numbers represent the percentage of cells within the indicated gate. (**e**) Quantification of T_{FH} (*top*) and T_H1 (*right*) – expressed as percentages of Ag-specific $CD4^+$ T cells out of total transferred cells – in dLNs of mice described in **d**. Mean+/- SEM is shown. *n=6 (rVSV), 8 (rLCMV).* Data are representative of at least 2 independent experiments. A one-way Anova with Bonferroni's post-test was applied. *** $p < 0.001$. (**f**) Quantification of the percentages of T_{FH} (*left*) and T_H1 (*right*) Ag-specific $CD4^+$ T cells (out of total transferred cells) in dLNs 5 days after infection of $CD45.2^+$ WT recipients injected with 1 x 10^6 purified $CD45.1^+$ Ag-specific (SMARTA) $CD4^+$ T cells and treated anti-IFNAR1 blocking antibody either 1 day prior to (light blue) or 1 day after (yellow) rVSV infection. Data are representative of at least 2 independent experiments. Mean +/- SEM is shown. *n=4.* A one-way Anova with Bonferroni's post-test was applied. ** $p < 0.01$; *** $p < 0.001$. (**g**) Quantification of the percentages of T_{FH} (*left*) and T_H1 (*right*) Ag-specific $CD4^+$ T cells (out of total transferred cells) in dLNs 5 days after infection (*bottom*) of $CD45.2^+$ WT recipients injected with 1 x 10^6 purified $CD45.1^+$ Ag-specific (SMARTA) $CD4^+$ T cells, infected with rLCMV and treated or not with Poly(I:C).. Data are representative of at least 2 independent experiments. PBS n=7, Poly(I:C) n=9. An unpaired two-tailed *t* test was applied. ** $p < 0.01$.

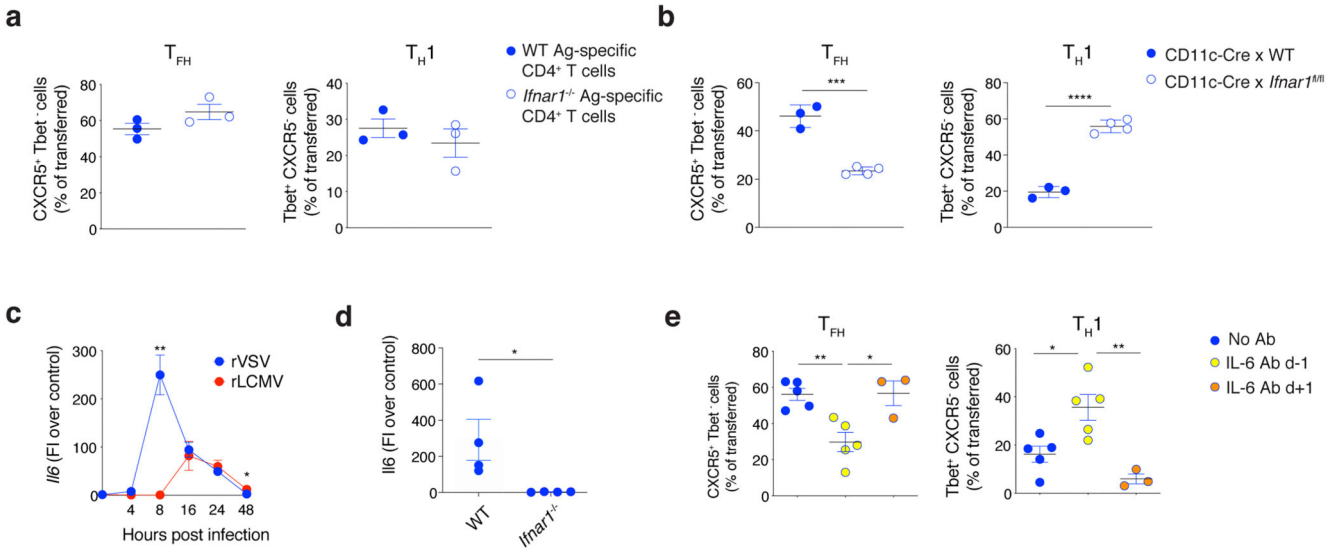

Fig. 4. Early type I IFN sensing by DC and IL-6 are essential for antiviral T_{FH} differentiation.

(**a**) Quantification of the percentages of T_{FH} and T_H1 Ag-specific $CD4^+$ T cells (out of total transferred cells) in dLNs 5 days after rVSV infection of $CD45.2^+$ WT mice injected with 1 x 10^6 purified $CD45.1^+$ WT or *Ifnar1*$^{-/-}$ Ag-specific (SMARTA) $CD4^+$ T cells. Mean +/- SEM is shown. *n*=3 (**b**) Quantification of the percentages of T_{FH} and T_H1 Ag-specific (SMARTA) $CD4^+$ T cells (out of total transferred cells) in dLNs 5 days after rVSV infection of either $CD45.2^+$ CD11c-Cre or $CD45.2^+$ CD11c-Cre x *Ifnar1*$^{fl/fl}$ recipients injected with 1 x 10^6 purified $CD45.1^+$ Ag-specific (SMARTA) $CD4^+$ T cells. dLNs were collected 5 days after rVSV infection. Data are representative of 3 independent experiments. Mean+/- SEM is shown. CD11c-Cre *n*=3, CD11c-Cre x *Ifnar1*$^{fl/fl}$ *n*=4. An unpaired two-tailed *t* test was applied. *** $p < 0.001$; **** $p < 0.0001$. (**c**) qPCR analysis of *Il6* gene expression profile at 0, 4, 8, 16, 24 and 48 hours in dLNs of rVSV (blue)- or rLCMV (red)-infected mice. Mean +/- SEM is shown. 0 hours *n* = 4; 4 hours *n* = 4; 8 hours *n* = 4; 16 hours *n* = 4; 24 hours *n* = 3 (rLCMV), 4 (rVSV); 48 hours *n* = 4. Data are pooled from 2 independent experiments. A two-way Anova with LSD post-test was applied. * $p < 0.05$; ** $p < 0.01$. (**d**) qPCR analysis of *Il6* gene expression in either wild-type or *Ifnar1*$^{-/-}$ mice in dLNs 8 hours after rVSV infection. Data are pooled from 2 independent experiments. Mean +/- SEM is shown. An unpaired two-tailed *t* test was applied. * $p < 0.05$. (**e**) Quantification of the percentages of T_{FH} (left) and T_H1 (right) Ag-specific $CD4^+$ T cells (out of total transferred cells) in $CD45.2^+$ wild-type recipients injected with 1 x 10^6 purified $CD45.1^+$ Ag-specific (SMARTA) $CD4^+$ T cells and treated with anti-IL-6 blocking antibody starting either 1 day prior to (yellow) or 1 day after rVSV infection (orange). Data are representative of at least 2 independent experiments. Mean +/- SEM is shown. No Ab *n*=5, IL-6 Ab d -1 *n*=5, IL-6 Ab d +1 *n*=3. A one-way Anova with Bonferroni's post-test was applied. * $p < 0.05$; ** $p < 0.01$.

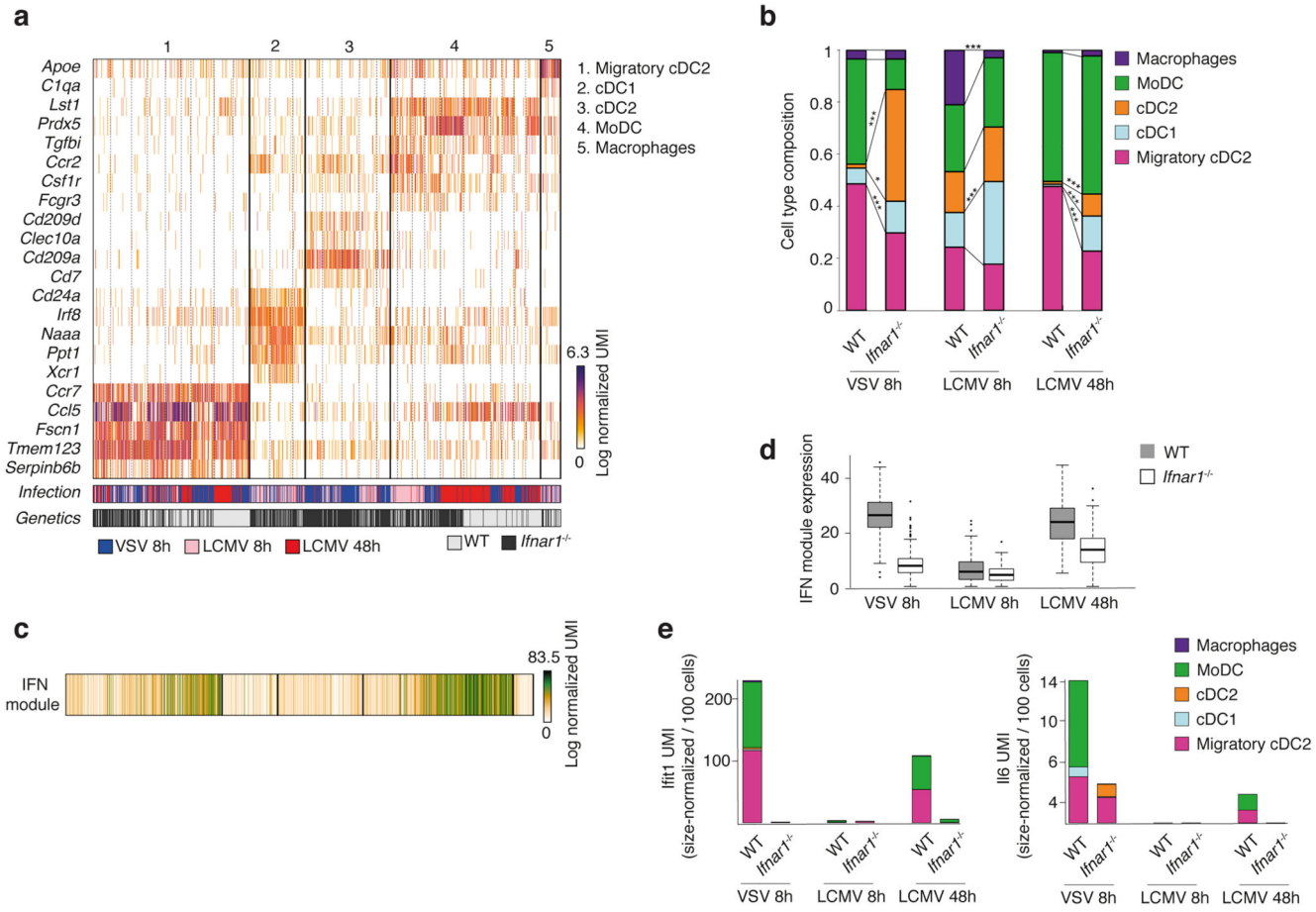

Fig. 5. scRNA-seq analysis of lymph node DCs upon viral infection.

(**a**) Gene expression profiles of 2179 single QC-positive lymph node CD11c^{+} MHC-II^{high} cells grouped in 5 clusters. The colour bars on the bottom indicates each cell's origin (blue: cells from the popliteal lymph node of mice 8 hours after intrafootpad rVSV infection; pink: cells from the popliteal lymph node of mice 8 hours after intrafootpad rLCMV infection; red: cells from the popliteal lymph node of mice 48 hours after intrafootpad rLCMV infection; light grey: WT mice; dark grey: *Ifnar1*$^{-/-}$ mice). **(b)** Relative abundance of different DC clusters 8 hours after rVSV infection, 8 hours after rLCMV infection and 48 hours after rLCMV infection. Dashed lines show changes in cluster abundances between WT and *Ifnar1*$^{-/-}$ mice under the same infection condition. Significant changes in abundances are highlighted. Two-sided FDR-adjusted Fisher's exact test. $*\ p < 0.05$; $***\ p < 0.001$ (**c**) Colour bar shows total size-normalized expression of interferon stimulated genes (ISGs) in cells in **(a).** Detailed expression of individual ISG genes is shown in Extended Data Fig. 10. (**d**) Distribution of total size-normalized expression of ISGs in CD11c^{+} MHC-II^{high} cells grouped by experimental condition. (**e**) Total expression of the ISG *Ifit1*, and the T_{FH} cell-promoting cytokine *Il6* in different experimental conditions. Values represent size-normalized total transcripts per 100 cells. Colours represent relative contribution from the five different DC subsets.

Europe PMC Funders Author Manuscripts